Loss of *Ezh2* synergizes with *JAK2*-V617F in initiating myeloproliferative neoplasms and promoting myelofibrosis

Takafumi Shimizu,[1] Lucia Kubovcakova,[1] Ronny Nienhold,[1] Jakub Zmajkovic,[1] Sara C. Meyer,[1] Hui Hao-Shen,[1] Florian Geier,[2] Stephan Dirnhofer,[3] Paola Guglielmelli,[4] Alessandro M. Vannucchi,[4] Jelena D. Milosevic Feenstra,[5] Robert Kralovics,[5] Stuart H. Orkin,[6,7,8] and Radek C. Skoda[1]

[1]Experimental Hematology, Department of Biomedicine, University Hospital Basel and University of Basel, 4031 Basel, Switzerland
[2]Bioinformatics Core Facility, Department of Biomedicine and [3]Institute of Pathology, University Hospital Basel, 4031 Basel, Switzerland
[4]Department of Clinical and Experimental Medicine, University of Florence, 50134 Florence, Italy
[5]CeMM Research Center for Molecular Medicine of the Austrian Academy of Sciences, 1090 Vienna, Austria
[6]Division of Hematology/Oncology, Boston Children's Hospital, Boston, MA 02115
[7]Department of Pediatric Oncology, Dana Farber Cancer Institute, Boston, MA 02215
[8]Howard Hughes Medical Institute, Harvard Medical School, Boston, MA 02215

Myeloproliferative neoplasm (MPN) patients frequently show co-occurrence of *JAK2*-V617F and mutations in epigenetic regulator genes, including *EZH2*. In this study, we show that *JAK2*-V617F and loss of *Ezh2* in hematopoietic cells contribute synergistically to the development of MPN. The MPN phenotype induced by *JAK2*-V617F was accentuated in *JAK2*-V617F;*Ezh2*$^{-/-}$ mice, resulting in very high platelet and neutrophil counts, more advanced myelofibrosis, and reduced survival. These mice also displayed expansion of the stem cell and progenitor cell compartments and a shift of differentiation toward megakaryopoiesis at the expense of erythropoiesis. Single cell limiting dilution transplantation with bone marrow from *JAK2*-V617F;*Ezh2*$^{+/-}$ mice showed increased reconstitution and MPN disease initiation potential compared with *JAK2*-V617F alone. RNA sequencing in *Ezh2*-deficient hematopoietic stem cells (HSCs) and megakaryocytic erythroid progenitors identified highly up-regulated genes, including *Lin28b* and *Hmga2*, and chromatin immunoprecipitation (ChIP)–quantitative PCR (qPCR) analysis of their promoters revealed decreased H3K27me3 deposition. Forced expression of *Hmga2* resulted in increased chimerism and platelet counts in recipients of retrovirally transduced HSCs. *JAK2*-V617F–expressing mice treated with an Ezh2 inhibitor showed higher platelet counts than vehicle controls. Our data support the proposed tumor suppressor function of *EZH2* in patients with MPN and call for caution when considering using Ezh2 inhibitors in MPN.

Myeloproliferative neoplasms (MPNs) are a group of diseases characterized by increased proliferation of erythroid, mega-karyocytic, and granulocytic lineages. Three clinical entities designated polycythemia vera (PV), essential thrombocythemia (ET), and primary myelofibrosis (MF [PMF]) are distinguished by clinical, laboratory, and molecular parameters (Tefferi et al., 2009). *JAK2*-V617F is the most frequently observed somatic mutation in MPN. This mutation augments the tyrosine kinase activity of *Jak2* and is found in >95% of patients with PV and in 50–60% of ET and PMF (Baxter et al., 2005; James et al., 2005; Kralovics et al., 2005; Levine et al., 2005). Other driver mutations are primarily associated with ET and PMF and target the genes for calreticulin, *CALR* (Klampfl et al., 2013; Nangalia et al., 2013), and the thrombopoietin receptor, *MPL* (Pardanani et al., 2006; Pikman et

al., 2006). Mutations in *JAK2*, *CALR*, and *MPL* are considered phenotypic driver mutations because they reproduce MPN phenotypes upon expression in mouse models. Genes encoding epigenetic regulators are also frequently mutated in MPN (Vainchenker et al., 2011). These mutations often coexist with one of the three driver gene mutations and are thought to promote clonal evolution and disease progression (Lundberg et al., 2014a). Mutations in the histone methyltransferase *EZH2* (*enhancer of zeste homologue 2*) are detected in 5–10% of patients with ET and PMF (Ernst et al., 2010) but are also found in other hematologic malignancies, including myelodysplastic syndromes and acute myeloid leukemia (Bejar et al., 2011; Gerstung et al., 2015). Patients with MPN carry either heterozygous or homozygous *EZH2* mutations (Ernst et al., 2010). Most of the *EZH2* mutations in MPN result in truncations of the Ezh2 protein and are therefore predicted to be loss of function mutations. In patients with MF, *EZH2* mutations are associated with poor prognosis (Guglielmelli et al., 2011).

The Rockefeller University Press $30.00
J. Exp. Med. 2016 Vol. 213 No. 8   1479–1496
www.jem.org/cgi/doi/10.1084/jem.20151136

CrossMark

1479

The Journal of Experimental Medicine

Several MPN mouse models have been established by expressing *JAK2*-V617F as transgenes or knock-in alleles (reviewed in Li et al. [2011]). Here we examined the effects of an *Ezh2* loss of function mutation in a Cre-recombinase–inducible mouse model of *JAK2*-V617F–driven MPN. These *JAK2*-V617F mice develop ET or PV phenotypes depending on the expression levels of *JAK2*-V617F in hematopoietic cells (Tiedt et al., 2008). Recently, we showed that hematopoietic stem cells (HSCs) expressing *JAK2*-V617F are capable of inducing clonal MPN in single cell transplantation (Lundberg et al., 2014b), albeit with low efficiency. This suggests that additional mutations, such as in *Ezh2*, may synergize with *JAK2*-V617F in MPN disease initiation.

Ezh2 functions as a core component of the polycomb repressive complex 2 (PRC2), which consists of three additional subunits, *Eed* (*embryonic ectoderm development*), *Suz12* (*suppressor of zeste 12 homologue*), and the histone binding protein *RBBP4*. PRC2 methylates lysine 27 on histone H3 (H3K27me3). *Ezh2* knockout mice are early embryonic lethal (O'Carroll et al., 2001), but several conditional knockout strains have been generated that allow inactivating *Ezh2* function in adult mice using inducible Cre-loxP systems (Hirabayashi et al., 2009; Neff et al., 2012). Conditional knockout of *Ezh2* in adult hematopoiesis has revealed that *Ezh2* is dispensable for the maintenance of long-term HSCs (LT-HSCs), most likely because of expression of *Ezh1*, a close homologue of *Ezh2* that associates with *Eed* and *Suz12* to form an alternative PRC2 complex that partially compensates for the loss of *Ezh2* (Xie et al., 2014). Here we studied *JAK2*-V617F and *Ezh2* double mutant mice in Cre-inducible conditional systems to assess the functional consequences in hematopoiesis.

RESULTS

To assess the functional effects of *Ezh2* loss on MPN phenotypes, we interbred mice with a conditional knockout allele of *Ezh2* (Neff et al., 2012) with inducible *JAK2*-V617F transgenic mice (hereafter called *V617F*; Tiedt et al., 2008). We first used the interferon-inducible *MxCre* system (Kühn et al., 1995) to delete one or both copies of *Ezh2* and simultaneously induce expression of *JAK2*-V617F. Heterozygous loss of *Ezh2* in *V617F* mice resulted in a trend toward more pronounced thrombocytosis and neutrophilia and initially also higher hemoglobin values than *V617F* alone (Fig. 1 A). *V617F* mice with homozygous loss of *Ezh2* exhibited elevated hemoglobin, thrombocytosis, and neutrophilia already at the time of induction by polyinosine-polycytosine (pIpC), consistent with leaky Cre expression. *V617F;Ezh2*$^{\Delta/\Delta}$ mice showed poor survival, whereas most of the *V617F;Ezh2*$^{+/\Delta}$ mice survived until they were sacrificed at 28 wk (Fig. 1 A, right). Loss of *Ezh2* in the absence of *V617F* had no effect on blood counts and did not affect survival. We repeated these experiments with the tamoxifen-inducible *SclCre*^{ER} system (Göthert et al., 2005). None of the mice showed an MPN phenotype before tamoxifen administration. The MPN phe-

notype appeared with a latency of ∼10 wk from the start of tamoxifen, and around this time the first deaths occurred (Fig. 1 B). Overall, the steepness of decline in survival of *V617F;Ezh2*$^{\Delta/\Delta}$ mice was comparable between *MxCre-* and *SclCre*-induced mice, although we cannot exclude that pIpC injections in *MxCre;V617F;Ezh2*$^{\Delta/\Delta}$ mice that already displayed MPN at the time of the injections might have had an additional negative impact on survival. The blood counts in *SclCre*-induced mice were comparable or slightly more pronounced than with the *MxCre* system (Fig. 1 B). *JAK2*-V617F with homozygous loss of *Ezh2* resulted in PMF without a preceding polycythemic phase. *Ezh2* mRNA expression was reduced to ∼50% in *Ezh2*$^{+/\Delta}$ mice and strongly decreased in *Ezh2*$^{\Delta/\Delta}$ mice (Fig. 1 C). This reduction was paralleled by a decrease in Ezh2 protein and histone H3 methylation on lysine 27 (H3K27me3; Fig. 1 D). Ubiquitination of histone H2A on lysine 119 (H2AK119Ub), a marker for the activity of the PRC1 complex, was not increased in *V617F;Ezh2*$^{\Delta/\Delta}$ mice. All mice expressing *V617F* displayed splenomegaly, but no differences were observed in *V617F* mice with or without *Ezh2* deletion (Fig. 1 E). Cellularity in BM was increased in *V617F* mice but markedly decreased in *V617F;Ezh2*$^{\Delta/\Delta}$ mice (Fig. 1 F). Furthermore, the numbers of circulating c-kit$^+$ progenitors cells were strongly increased in *V617F;Ezh2*$^{\Delta/\Delta}$ mice (not depicted). The decrease in BM cellularity with an increase in circulating progenitor cells and a fall in hemoglobin over time in *V617F;Ezh2*$^{\Delta/\Delta}$ mice is compatible with MF and is reminiscent of changes typically observed in patients with PMF with increased numbers of circulating CD34$^+$ cells (Barosi et al., 2001). At 16 wk, all *V617F* mice, with or without *Ezh2* loss, showed typical histopathological features of MPN, with trilineage hyperplasia and increased numbers of atypical megakaryocytes, together with destruction of normal splenic architecture by infiltrates of highly atypical hematopoiesis (Fig. 1, G and H). Loss of *Ezh2* in *V617F* mice accentuated the hyperproliferation of the megakaryocytic lineage and resulted in a marked increase in reticulin fibers in BM and spleen, most prominently seen in *V617F;Ezh2*$^{\Delta/\Delta}$ mice, which also displayed an increase in collagen fibers and osteosclerosis (not depicted). These changes were not observed in *Ezh2*$^{+/\Delta}$ or *Ezh2*$^{\Delta/\Delta}$ mice with WT *Jak2*. Thus, heterozygous loss of *Ezh2* accelerated the transition from PV to MF and homozygous loss of *Ezh2* appears to directly lead to PMF, without a preceding polycythemic phase. None of the mice showed transformation to acute leukemia.

Analysis of the progenitor and stem cell compartments by flow cytometry revealed an increase of phenotypic LT-HSCs and short-term HSCs (ST-HSCs) in BM and spleen of all genotypes expressing *V617F* (Fig. 2 A). Furthermore, multipotential progenitors (MPPs) and lineage-negative Sca-1$^+$ c-kit$^+$ (LSK) cells were increased in spleen, while a trend toward increased LSKs was also noted in BM (Fig. 2 A). Heterozygous deletion of *Ezh2* on the *V617F* background increased LT-HSCs in BM and spleen, whereas homozygous deletion of *Ezh2* on the *V617F* background was associated with in-
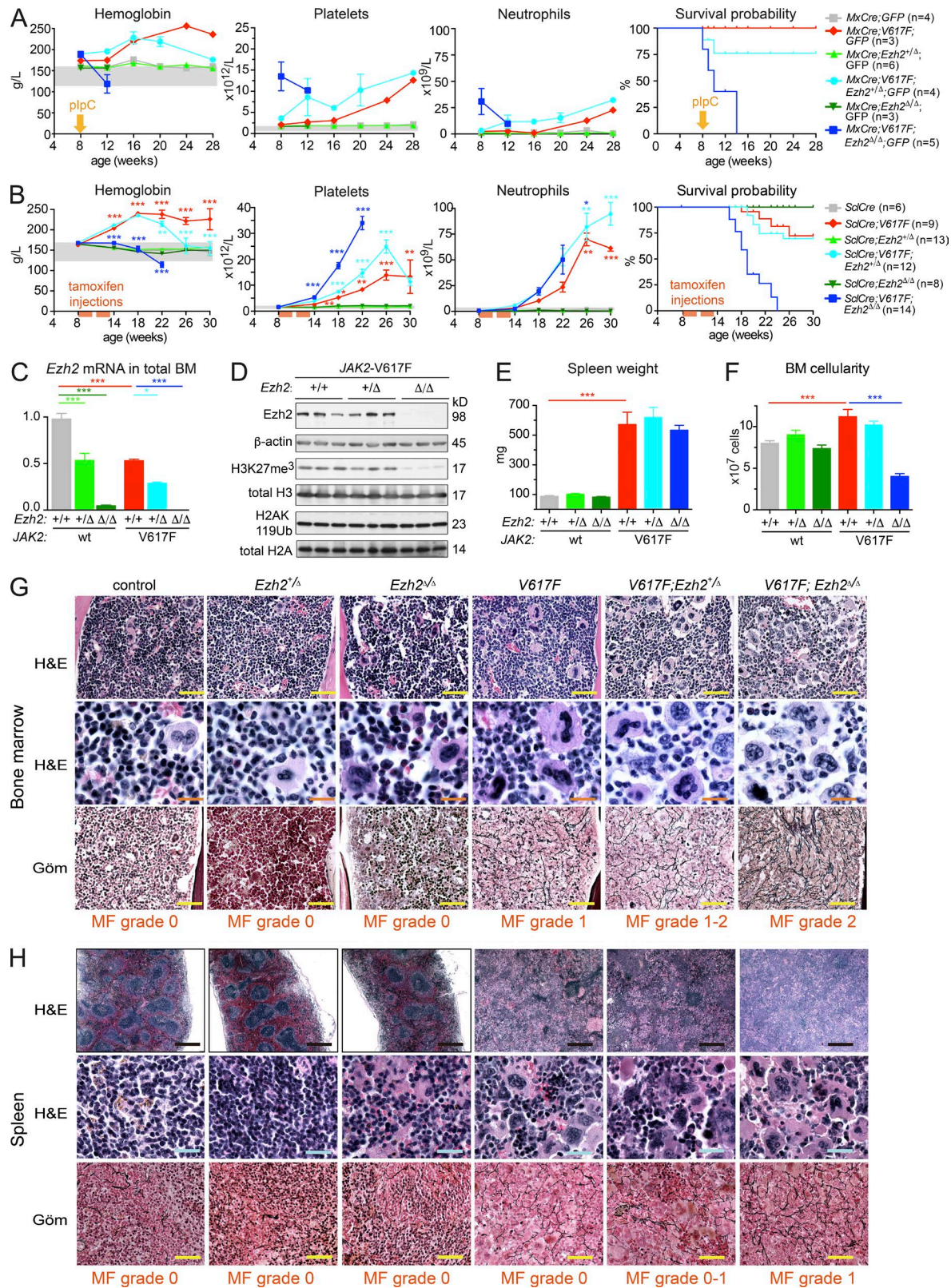
Figure 1. **Analysis of *V617F;Ezh2* double mutant mice.** (A) Time course of blood counts and survival of *MxCre* mice induced with pIpC (yellow arrows). The color code for the different genotypes is the same as indicated in C–F. The gray horizontal bars indicate the normal range for the blood values. Survival probability was calculated by the Kaplan-Meier method. The means of the values ± SEM are plotted (*n* = 4 for *MxCre;GFP, n* = 6 for *MxCre;Ezh2^{+/Δ};GFP,*

creased LT-HSCs in spleen and increased ST-HSCs in BM and MPPs in spleen (Fig. 2 A). Loss of *Ezh2* on WT *Jak2* background caused no significant changes in the HSC compartments. Analysis of the more mature progenitor compartments (Fig. 2 B) showed that *V617F* alone increased megakaryocyte progenitors (MkPs) and megakaryocytes in spleen, whereas a prominent decrease in erythroid precursors occurred in BM, compensated by a strong increase of erythroid precursors in spleen (Fig. 2 B). Homozygous loss of *Ezh2* displayed a significant increase of MkPs and megakaryocytes and also megakaryocyte erythroid progenitors (MEPs) but decreased erythroid precursors in spleen (Fig. 2 B). Thus, heterozygous and homozygous loss of *Ezh2* on *V617F* background expanded the early HSC and progenitor compartment and favored megakaryopoiesis over erythropoiesis. Plasma levels of Tpo were decreased in mice expressing *V617F* compared with mice expressing WT *Jak2* (Fig. 2 C). Loss of *Ezh2* on *V617F* background further reduced the Tpo plasma levels, consistent with autoregulation of Tpo by the increased platelet and megakaryocyte mass. Interestingly, TGFβ in plasma showed a trend toward the highest levels in *V617F;Ezh2*$^{\Delta/\Delta}$ mice, consistent with the role of TGFβ as a mediator of MF.

To eliminate potential effects of *Ezh2* deletion in nonhematopoietic tissues and to determine how the double mutant cells compete with WT hematopoiesis, we transplanted noninduced LSK cells together with WT BM competitor cells (Fig. 3). To allow monitoring of hematopoietic cells that carry the *JAK2* and/or *Ezh2* mutations, we crossed these strains with the *UBC-GFP* strain (Schaefer et al., 2001) and obtained donor mice that coexpressed GFP in the same cells (*V617F;GFP* or *V617F;Ezh2;GFP*). Both *V617F;Ezh2*$^{+/\Delta}$ and *V617F;Ezh2*$^{\Delta/\Delta}$ mice showed a competitive advantage in the platelet and neutrophil lineages compared with *V617F* mice, whereas the differences in the erythroid lineage were minor (Fig. 3 A). The same conclusions were reached in competitive transplantations of BM cells from *SclCre;V617F;GFP* mice with heterozygous and homozygous loss of *Ezh2* (Fig. 3 B).

To determine whether loss of *Ezh2* also synergizes with *JAK2*-V617F in MPN disease initiation from single cells, we performed competitive transplantations at limiting dilutions (Fig. 4). We used the approach previously established for studying *V617F* mice (Lundberg et al., 2014b). Because the majority of MPN patients with *Ezh2* mutations remain heterozygous and the *V617F;Ezh2*$^{\Delta/\Delta}$ mice show early lethality, we performed limiting dilutions with BM cells from heterozygous *V617F;Ezh2*$^{+/\Delta}$ mice (Fig. 4 A). The numbers of phenotypic LT-HSCs in *V617F* and *V617F;Ezh2*$^{+/\Delta}$ mice were increased two- to threefold compared with WT controls (Fig. 4 B). To obtain on average one HSC per transplant, we therefore reduced the number of BM cells from *MxCre;V617F;GFP* and *MxCre:V617F;Ezh2*$^{+/\Delta}$*;GFP* donor mice to 8,000 cells per recipient, whereas 20,000 cells were used for the other genotypes. The time course of the blood counts and chimerism is summarized in Fig. 4 C. Data for each genotype was arranged in vertical columns. The frequencies of reconstitution, defined as chimerism >1% in Gr1-positive peripheral blood cells 22 wk after transplantation, are summarized in Table 1. Recipients of limiting dilutions of BM cells from *V617F;GFP* mice showed a high degree of trilineage chimerism, but only a few of them developed MPN phenotype with mostly ET characteristics. The recipients of BM from *V617F;Ezh2*$^{+/\Delta}$*;GFP* mice reconstituted at higher frequencies and in most cases showed a PV phenotype (Fig. 4 C and Table 1). Recipients of *Ezh2*$^{+/\Delta}$*;GFP* BM with WT *Jak2* showed increased frequency of reconstitution (Table 1), but only few of them showed chimerism above 20% (Fig. 4 C). BM cellularity between *V617F* and *V617F;Ezh2*$^{+/\Delta}$ mice was comparable (Fig. 4 D), but only the *V617F;Ezh2*$^{+/\Delta}$ mice displayed splenomegaly (Fig. 4 E). In line with our previous study (Lundberg et al., 2014b), analysis of the percentages of the *V617F;GFP*-positive cells in hematopoietic progenitor and stem cell compartments in BM revealed that mice with MPN phenotype retained a high degree of *GFP* chimerism in the LT-HSC compartment, in contrast to mice without MPN

n = 3 for *MxCre;Ezh2*$^{\Delta/\Delta}$*;GFP*, *n* = 3 for *MxCre;V617F;GFP*, *n* = 4 for *MxCre;V617F;Ezh2*$^{+/\Delta}$*;GFP*, and *n* = 5 for *MxCre;V617F;Ezh2*$^{\Delta/\Delta}$*;GFP*). (B) Analysis of *V617F;Ezh2* double mutant mice using the inducible *SclCre* system. Time course of blood counts of mice induced with tamoxifen injections for 5 wk with 1-wk break (orange horizontal bars). The means of the values ± SEM are plotted (*n* = 6 for *SclCre*, *n* = 13 for *SclCre;Ezh2*$^{+/\Delta}$, *n* = 8 for *SclCre;Ezh2*$^{\Delta/\Delta}$, *n* = 9 for *SclCre;V617F*, *n* = 12 for *SclCre;V617F;Ezh2*$^{+/\Delta}$, and *n* = 14 for *SclCre;V617F;Ezh2*$^{\Delta/\Delta}$). The same color code for the different genotypes is used. (C) A subset of mice was sacrificed at 12 wk after tamoxifen induction. Expression of *Ezh2* mRNA was determined by real-time PCR in total BM and is shown in arbitrary units with WT (wt) control BM set to the value of 1. The group sizes were *n* = 5 for *SclCre*, *n* = 5 for *SclCre;Ezh2*$^{+/\Delta}$, *n* = 4 for *SclCre;Ezh2*$^{\Delta/\Delta}$, *n* = 4 for *SclCre;V617F*, *n* = 5 for *SclCre;V617F;Ezh2*$^{+/\Delta}$, and *n* = 5 for *SclCre;V617F;Ezh2*$^{\Delta/\Delta}$. (D) Western blots of total BM cell lysates probed with antibodies against Ezh2, β-actin, H3K27me3, total histone H3, H2AK119Ub, and total H2A are shown. Genotypes are indicated above the corresponding lanes (*n* = 3 for each group). This experiment was performed twice. (E and F) Spleen weight (E) and BM cellularity (F) are shown at 12 wk after tamoxifen (*n* = 9 or 12 for *SclCre*, *n* = 7 or 12 for *SclCre;Ezh2*$^{+/\Delta}$, *n* = 10 or 13 for *SclCre;Ezh2*$^{\Delta/\Delta}$, *n* = 5 or 8 for *SclCre;V617F*, *n* = 6 or 10 for *SclCre;V617F;Ezh2*$^{+/\Delta}$, and *n* = 6 or 8 for *SclCre;V617F;Ezh2*$^{\Delta/\Delta}$ for spleen weight or BM cellularity). This experiment was performed four times. (C, E, and F) Results are presented as means ± SEM. (G and H) Histopathology of BM and spleen taken at 16 wk after start of tamoxifen injection. The sections were stained with hematoxylin and eosin (H&E) or with the Gömöri stain (Göm). The grade of MF is indicated under the corresponding pictures. Grading of MF was performed on three mice per group, and one representative mouse per genotype is shown. Bars: (black) 500 µm; (yellow) 50 µm; (blue) 20 µm; (orange) 10 µm. Statistical analysis was conducted using the Student's *t* test or one-way ANOVA with Bonferroni's post-hoc multiple comparison test. *, P < 0.05; **, P < 0.01; ***, P < 0.001. Red asterisks indicate significance between control and *V617F*. Light blue asterisks indicate significance between *V617F* and *V617F;Ezh2*$^{+/\Delta}$. Dark blue asterisks indicate significance between *V617F* and *V617F;Ezh2*$^{\Delta/\Delta}$.
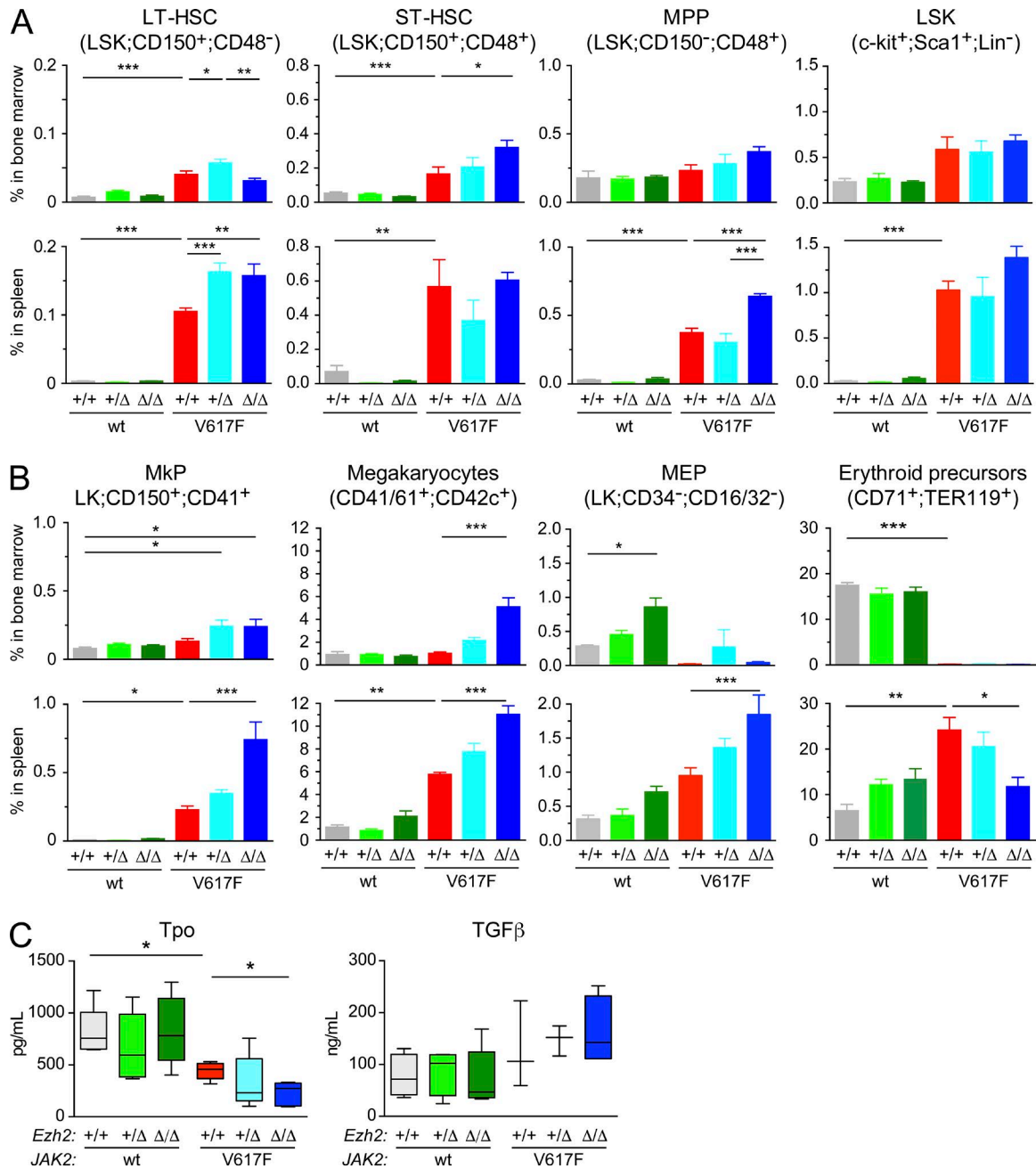
Figure 2. Flow cytometric analysis of stem cell and progenitor compartments in BM and spleen of tamoxifen–inducible _JAK2_–V617F and _Ezh2_ mutant mice. (A) Frequencies of LT-HSCs, ST-HSCs, MPPs, and LSK cells are shown. The top panel shows analysis of BM, and the bottom panel analysis of spleen cells for the different genotypes, as indicated (_n_ = 5 for _SclCre_, _n_ = 4 for _SclCre;Ezh2_$^{+/\Delta}$, _n_ = 6 for _SclCre;Ezh2_$^{\Delta/\Delta}$, _n_ = 6 for _SclCre;V617F_, _n_ = 4 for _SclCre;V617F;Ezh2_$^{+/\Delta}$, and _n_ = 4 for _SclCre;V617F;Ezh2_$^{\Delta/\Delta}$) This experiment was performed three times. (B) Frequencies of MkPs, megakaryocytes, MEPs, and erythroid precursors are shown for BM (top) and spleen (bottom). The same mice as in A were analyzed. (C) Plasma concentrations of Tpo and TGFβ from tamoxifen-inducible _JAK2_-V617F and _Ezh2_ mutant mice were measured by ELISA (_n_ = 5 per group for TPO; _n_ = 4 for _SclCre_, _n_ = 4 for _SclCre;Ezh2_$^{+/\Delta}$, _n_ = 5 for _SclCre;Ezh2_$^{\Delta/\Delta}$, _n_ = 3 for _SclCre;V617F_, _n_ = 3 for _SclCre;V617F;Ezh2_$^{+/\Delta}$, and _n_ = 5 for _SclCre;V617F;Ezh2_$^{\Delta/\Delta}$ for TGFβ). Statistical analysis was conducted using the Student's _t_ test or one-way ANOVA with Bonferroni's post-hoc multiple comparison test. *, P < 0.05; **, P < 0.01; ***, P < 0.001. Results are presented as means ± SEM.
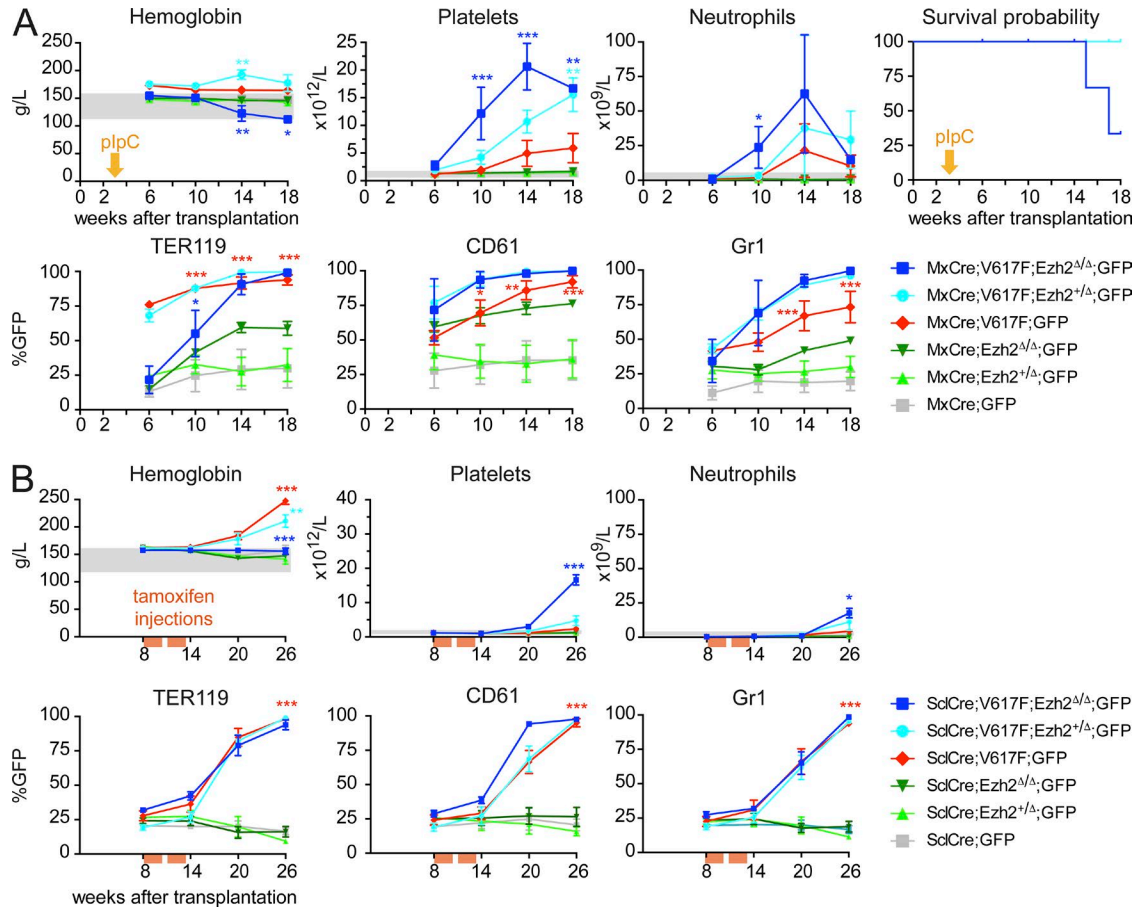
Figure 3. **Competitive BM transplantations.** (A) Transplantation of noninduced LSK cells (1,500 FACS-sorted cells) from *MxCre* mouse mutants coexpressing *GFP* mixed with WT BM cells (1.5×10^6). Time course of blood counts and survival of transplanted mice after induction with pIpC (yellow arrows) are shown in the top panel. The bottom panel shows the chimerism assessed by the percentage of GFP-positive cells for the erythroid (TER119), platelet (CD61), and granulocytic (Gr1) lineages. The experiment was performed twice. One experiment is shown with *n* = 5 for *MxCre;GFP*, *n* = 5 for *MxCre;Ezh2^+/Δ;GFP*, *n* = 3 for *MxCre;Ezh2^Δ/Δ;GFP*, *n* = 5 for *MxCre;V617F;GFP*, *n* = 5 for *MxCre;V617F;Ezh2^+/Δ;GFP*, and *n* = 3 for *MxCre;V617F;Ezh2^Δ/Δ;GFP*. (B) Competitive transplantation with noninduced *SclCre* mutant BM cells coexpressing GFP (0.25×10^6) mixed at 1:3 ratio with WT BM cells (0.75×10^6). Activation of *V617F* and knockout of the floxed *Ezh2* alleles were induced with tamoxifen injections for 5 wk with 1-wk break (orange horizontal bars). The time course of the blood counts (top) and the corresponding chimerism in peripheral blood (bottom) are shown (*n* = 8 for *SclCre*, *n* = 8 for *SclCre;Ezh2^+/Δ*, *n* = 8 for *SclCre;Ezh2^Δ/Δ*, *n* = 6 for *SclCre;V617F*, *n* = 6 for *SclCre;V617F;Ezh2^+/Δ*, and *n* = 6 for *SclCre;V617F;Ezh2^Δ/Δ*). Statistical analysis was conducted using one-way ANOVA with Bonferroni's post-hoc multiple comparison test. *, P < 0.05; **, P < 0.01; ***, P < 0.001. Red asterisks indicate significance between control and *V617F*. Light blue asterisks indicate significance between *V617F* and *V617F;Ezh2^+/Δ*. Dark blue asterisks indicate significance between *V617F* and *V617F;Ezh2^Δ/Δ*. Gray horizontal bars indicate the normal range for C57BL/6 mice. Results are presented as means ± SEM.

phenotype, where the expansion of *V617F;GFP* chimerism often occurred at later stages of differentiation (Fig. 4 F). The same pattern was also observed in three out of four of the *V617F;Ezh2^+/Δ;GFP* mice with MPN phenotype that were analyzed (Fig. 4 F, right). This suggests that in some cases heterozygous loss of *Ezh2* may help to overcome restrictions that prevent developing MPN when the *V617F* clone has not fully expanded in the LT-HSC compartment. Overall, these results show that heterozygous loss of *Ezh2* synergized with *V617F* also in monoclonal MPN disease initiation at limiting dilutions.

To further examine the effects of the *Ezh2* mutations on the LT-HSC compartment, we transplanted 50 LT-HSCs

purified by FACS sorting from donor mice taken 12 wk after tamoxifen induction and assessed their functional capacity to reconstitute and initiate MPN in lethally irradiated recipients (Fig. 5). We used 10^6 WT BM cells as competitors (Fig. 5 A). Because of reduced survival of mice reconstituted with *V617F;Ezh2^Δ/Δ;GFP* BM, we terminated the experiment at 24 wk and the results of analysis at 16 wk are shown (Fig. 5 B). Only 4/10 recipients (40%) that received purified LT-HSCs from *V617F;GFP* reconstituted with a chimerism of >1% in Gr1-positive cells, and only 2 of the chimeric mice also showed an MPN phenotype. This result confirms our previous findings, which showed that the functional stem cell compartment in *V617F* mice is shifted toward cells with a
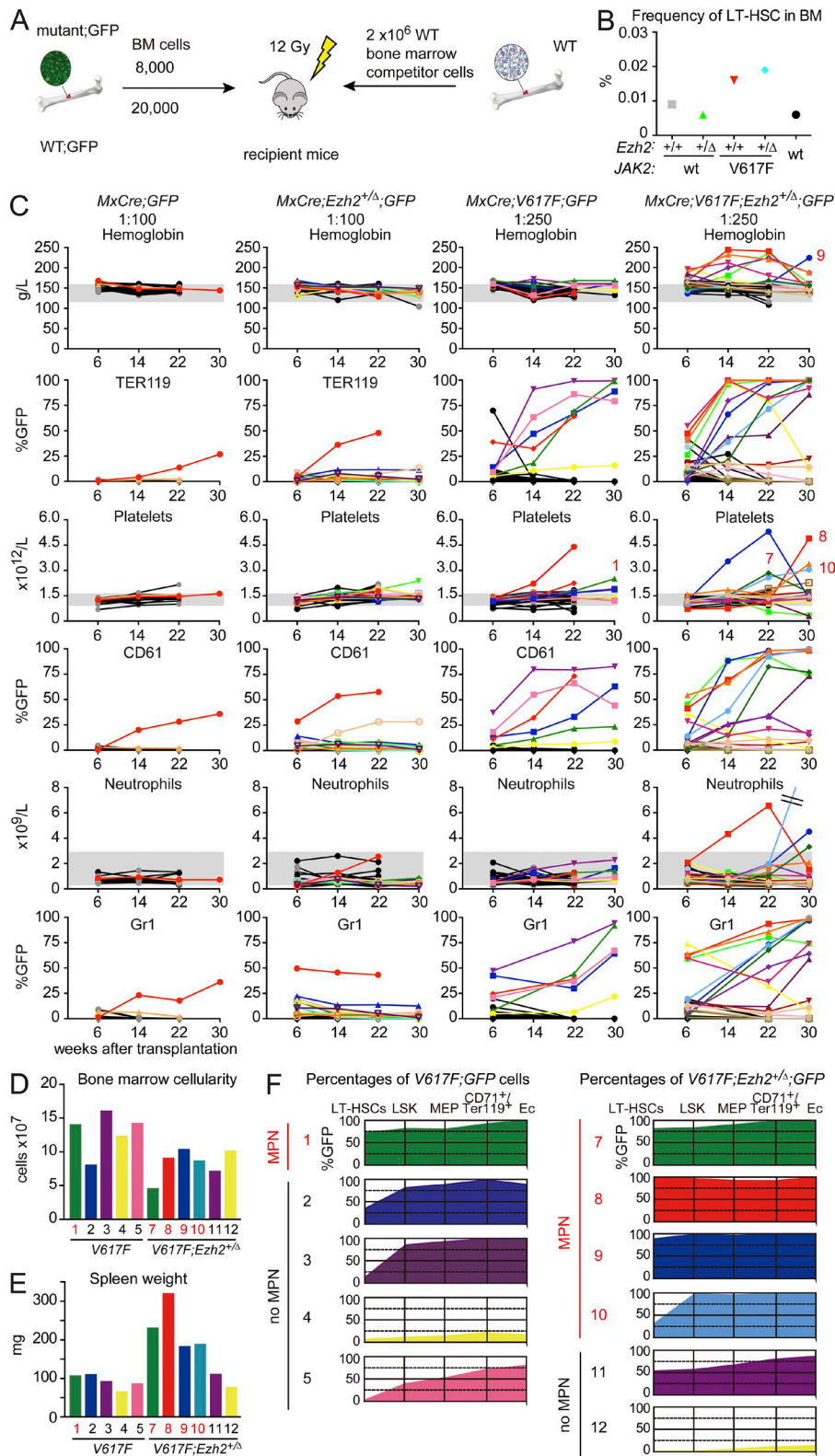
Figure 4. Competitive limiting dilution transplantations of BM cells from mouse mutants. (A) The schematic drawing shows the design of the experiment. (B) The frequency of phenotypic LT-HSCs was determined by flow cytometry in the individual donor mice that were previously induced with pIpC 5 wk before the transplantation. (C) Time course of blood counts and chimerism determined by GFP in peripheral blood is shown for the four different genotypes as indicated. This experiment was performed once with a total of 141 recipient mice. Individual mice showing chimerism >1% at 22 wk in Gr1-positive lineage are shown with colored symbols and lines ($n = 19$ for *MxCre;GFP*, $n = 40$ for *MxCre;Ezh2+/Δ;GFP*, $n = 41$ for *MxCre;V617F;GFP*, and $n = 41$ for *MxCre;V617F;Ezh2+/Δ;GFP*). Gray horizontal bars indicate the normal range for C57BL/6 mice. (D and E) BM cellularity (D) and spleen weights (E) of five *V617F* and six *V617F;Ezh2+/Δ* mice at 30 wk after transplantation. Numbers in red indicate mice with the MPN phenotype, and numbers in black are mice without the MPN phenotype. (F) Graph showing the evolution of *V617F;GFP* and *V617F;Ezh2+/Δ;GFP* cells at different stages of HSC, progenitor, or erythroid cell differentiation. These mice were sacrificed 30 wk after transplantation. The percentages of GFP cells indicate the size of the mutant clone (colored area). The mice with the MPN phenotype are also identified by their numbers in red color in the hemoglobin or platelet charts in C. CD71+/TER119+, erythroid precursor cells; Ec, erythrocytes.

lineage-intermediate immunophenotype (Lundberg et al., 2014b). Interestingly, heterozygous loss of *Ezh2* on *V617F* background increased the frequency of reconstitution to 5/9

recipients (56%), and 4/5 mice with chimerism also displayed an MPN phenotype (Fig. 5 B). The effect of homozygous loss of *Ezh2* on *V617F* background was even more pronounced,

Table 1. Summary of competitive limiting dilution transplantation experiments

Genotype of donor mice	Recipients n =	Number of BM cells transplanted	Frequency of long-term reconstitution[a]	Mice with MPN phenotype
MxCre;GFP	19	20,000	2/19 (10%)	0
MxCre;Ezh2+/Δ;GFP	40	20,000	13/40 (32.5%)	1/13 (7.6%)
MxCre;V617F;GFP	41	8,000	6/41 (15%)	2/6 (33%)
MxCre;V617F;Ezh2+/Δ;GFP	41	8,000	16/41 (39%)	8/16 (50%)

The indicated numbers of BM cells were injected into lethally irradiated recipients.
[a]Reconstitution was scored based on the presence of >1% GFP-positive cells in the peripheral blood Gr1+ cells at 22 wk after transplantation.

and 9/9 recipient showed high chimerism and displayed an ET phenotype (Fig. 5 B), while their survival was reduced (Fig. 5 C). The frequencies of reconstitution and MPN disease initiation is summarized in Fig. 5 D. Homozygous loss of *Ezh2* on *Jak2* WT background reduced the frequency of reconstitution (5/8 recipients) compared with WT BM cells (8/9 recipients), but at the same time resulted in a shift toward higher percentage of myeloid cells in peripheral blood (Fig. 5 E). *V617F* alone also resulted in a myeloid bias, and the combination of *V617F;Ezh2*$^{Δ/Δ}$ shifted the percentages almost completely toward myeloid cells (Fig. 5 E). Comparison of the platelet and erythrocyte chimerisms in peripheral blood for all recipients of BM from *Ezh2* mutants on *Jak2* WT background is shown in Fig. 5 F. Homozygous loss of *Ezh2* alone already leads to a shift toward thrombopoiesis.

To study the mechanism of how loss of *Ezh2* contributes to enhancement of the MPN phenotype, we compared the mRNA expression profiles of hematopoietic cells with or without mutations in *JAK2* and *Ezh2* by RNA sequencing. LT-HSCs and MEP cells were FACS sorted from groups of four to six mice per genotype 10 wk after tamoxifen induction, and RNA was used to prepare libraries for sequencing on Illumina NextSeq500. The mutant versus WT Jak2 is the dominant parameter that divides the heat map of LT-HSCs into two groups (Fig. 6 A), and this influence is also represented in the principal component analysis (PCA) along the principal component 1 axis (Fig. 6 B, left). In MEPs, the influence of the Jak2 genotype is less prominent. Instead, unsupervised clustering reveals a strong influence of the homozygous loss of Ezh2, which defines two distinct groups in the heat map, one with WT Jak2 and one with V617F (Fig. 6 A, right). The effects of heterozygous loss of *Ezh2* were less prominent in the clustering and the groups of *V617F* and *V617F;Ezh2*$^{+/Δ}$ MEPs appear to be rather heterogeneous. In PCA of the MEP data, WT *Jak2* versus *V617F* is the dominant factor (principal component 1), explaining 43% of the variation in log2-fold change (Fig. 6 B, right). The second most prominent effect in the PCA (principal component 2) is observed between homozygous loss of *Ezh2* versus heterozygous or WT *Ezh2*, which accounts for 21% of the variation in log2-fold change. Competitive gene set enrichment analysis comparing LT-HSCs from *V617F;Ezh2*$^{Δ/Δ}$ versus *V617F* mice revealed interferon-γ and interferon-α signatures (Fig. 6 C). Using self-contained gene set testing, we also found posi-

tive enrichment of a fetal liver HSC-specific gene signature (Fig. 6 C, right). In LT-HSCs, the largest number of differentially expressed genes was found between WT cells and cells expressing V617F (Fig. 6 D). There are fewer differentially expressed genes in *V617F*-expressing cells with different *Ezh2* genotypes, and homozygous loss of *Ezh2* had a much stronger effect than heterozygous loss. Few differences in gene expression were detected between different *Ezh2* genotypes on a WT *Jak2* background. In MEPs, the largest number of differentially expressed genes (with P ≤ 0.05) is observed in genotypes that involve comparisons with homozygous loss of *Ezh2* both on WT *Jak2* and *V617F* background (Fig. 6 D). The second largest effect is seen in the comparison between *V617F* and WT *Jak2*, whereas the heterozygous *Ezh2* showed the fewest changes both in comparison with WT *Jak2* and in comparison between *V617F* and *V617F;Ezh2*$^{+/Δ}$. The top 10 differentially expressed genes for the comparisons between WT and *Ezh2*$^{Δ/Δ}$ and *V617F* with *V617F;Ezh2*$^{Δ/Δ}$ were ordered according to the absolute fold change in expression and are shown in Fig. 6 E. There was no overlap among the top 10 gene lists from LT-HSCs and MEP, except for *Lin28b*, which showed the highest fold changes in both LT-HSCs and MEPs. The complete list of differentially expressed genes is provided in Tables S1 and S2. *Lin28b*, together with *let-7* and *Hmga2*, plays an important role in regulating HSC self-renewal (Oguro et al., 2012; Copley et al., 2013). The log2 expression levels of *Lin28b* and its downstream gene *Hmga2* are plotted in Fig. 6 F. In LT-HSCs, *Lin28b* was significantly elevated only in *V617F;Ezh2*$^{Δ/Δ}$ cells, whereas in MEPs both WT *Jak2;Ezh2*$^{Δ/Δ}$ and *V617F;Ezh2*$^{Δ/Δ}$ cells showed increased *Lin28b* (Fig. 6 F). *Hmga2* expression was unchanged in LT-HSCs (not depicted). However, *Hmga2* expression was significantly elevated in MEPs from mice with *Ezh2*$^{Δ/Δ}$ on WT *Jak2* or *V617F* backgrounds (Fig. 6 F, right).

Up-regulated expression of *Hmga2* was previously linked to increased megakaryopoiesis and MF (Oguro et al., 2012). We determined the mRNA expression levels of *HMGA2* in granulocytes from MPN patients with *EZH2* mutations (Fig. 6 G). A trend toward higher expression of *HMGA2* was observed in four patients with mutations in *CALR* that carried heterozygous *EZH2* mutations and were very high in one patient with mutated CALR and a homozygous *EZH2* mutation. Patients with *JAK2*-V617F and homozygous *EZH2* mutations also showed a trend toward higher *HMGA2* expression. We also

1486

Synergism between *Ezh2* deficiency and *JAK2*-V617F | Shimizu et al.
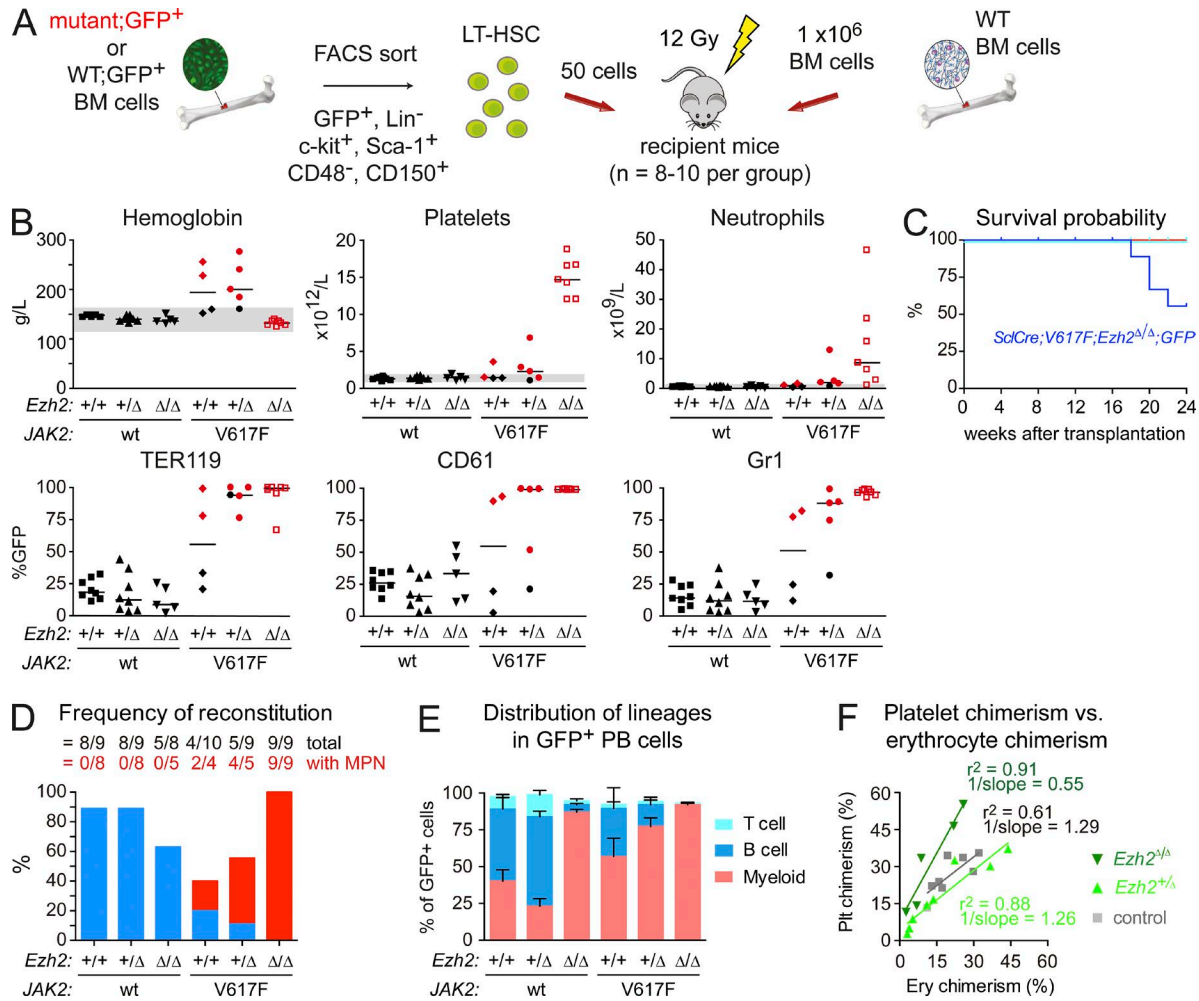
Figure 5. **Competitive transplantation of purified LT–HSCs.** (A) Schematic drawing shows the design of the experiment. The donor mice were induced with tamoxifen 10 wk before they were sacrificed. LT-HSCs were isolated using FACS with the antibodies as indicated. For transplantation, 50 mutant LT-HSCs coexpressing GFP were mixed with 10^6 WT BM cells and injected into lethally irradiated recipient mice. The experiment was performed twice with a total of 79 recipient mice. One experiment with $n = 9$ for *SclCre;GFP*, $n = 9$ for *SclCre;Ezh2$^{+/\Delta}$;GFP*, $n = 8$ for *SclCre;Ezh2$^{\Delta/\Delta}$;GFP*, $n = 10$ for *SclCre;V617F;GFP*, $n = 9$ for *SclCre;V617F;Ezh2$^{+/\Delta}$;GFP*, and $n = 9$ for *SclCre;V617F;Ezh2$^{\Delta/\Delta}$;GFP* is shown. (B) Blood counts and GFP chimerism of BM chimera mice at 16 wk after transplantation are shown. Individual mice that displayed the MPN phenotype are marked in red color. Horizontal lines indicate the mean of the values. Gray horizontal bars indicate the normal range for C57BL/6 mice. (C) Survival probability was calculated by the Kaplan-Meier method. (D) Analysis of reconstitution by the mutant LT-HSCs. The bars represent the percentages of reconstitution, assessed by GFP for each of the genotypes. Failure to reconstitute was defined as <1% GFP-positive cells in the Gr1 lineage in the peripheral blood at 16 wk after transplantation. Blue bars indicate reconstitution without the MPN phenotype, whereas red portions of the bars indicate the proportion of mice with the MPN phenotype. (E) Analysis of lineage distribution in GFP-positive cells in peripheral blood. Results are presented as means ± SEM. (F) Correlation between platelet (Plt) chimerism and erythroid (Ery) chimerism in peripheral blood of mice with *Ezh2* mutations on WT *Jak2* background.

examined expression of two other genes in patients' granu-locytes: *IGF2BP3*, a downstream target of *Lin28b* pathway, and *Pcolce2*, an up-regulated gene in the top 10 list of MEPs from mice with *Ezh2$^{\Delta/\Delta}$* on WT and *V617F* backgrounds. Both showed a similar trend toward higher expression in MPN patients with *EZH2* mutations. These data are consistent with a model in which the decrease of PRC2 activity through loss of *Ezh2* ultimately results in gene expression changes that favor megakaryopoiesis but alone are insufficient to cause a thrombocytosis phenotype, unless *JAK2*-V617F is coexpressed.

The *Lin28b–Let7–Hmga2* axis is an attractive candidate pathway to mediate the synergistic effect of loss of *Ezh2* and expression of *JAK2*-V617F and on megakaryopoiesis. To de-termine whether the promoters of *Lin28b* and *Hmga2* are directly affected by the loss of Ezh2 activity, we performed chromatin immunoprecipitation (ChIP) with antibodies against H3K27me3 followed by quantitative PCR (qPCR) analysis using primers for the promoter regions of *Lin28b* and *Hmga2* (Fig. 7 A). We found that both the *Lin28b* and *Hmga2* promoters exhibited significantly reduced H3K27me3 depo-
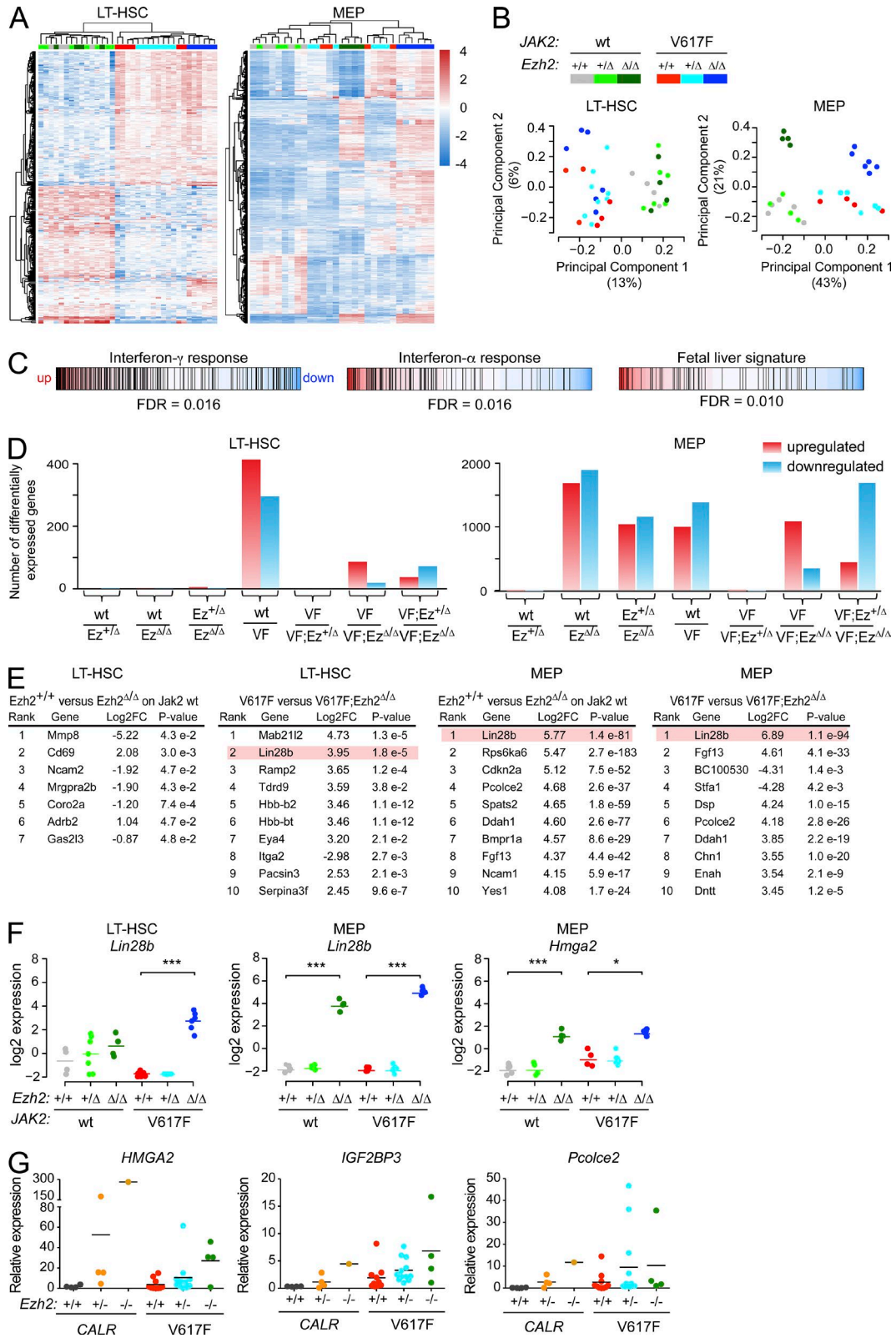
Figure 6. Gene expression analysis by RNA sequencing of LT–HSCs and MEPs. (A) Unsupervised clustering of differentially expressed genes (P ≤ 0.05; log2-fold changes >1.5). Each column represents data from one individual mouse. The color code for the genotypes of the individual mice is the same as in B. (B) PCA. The data for LT-HSCs and MEPs were derived from two independent experiments and combined (*n* = 4 or 5 for *SclCre*, *n* = 7 or 4 for

sition in sorted LSK and MEP cells from $Ezh2^{\Delta/\Delta}$ mice, suggesting that both are directly affected by the loss of $Ezh2$. Next, we examined the effects of forced expression of $Lin28b$ or $Hmga2$ in vitro by retroviral transduction and culture of FACS-sorted LT-HSCs from WT or V617F-expressing BM (Fig. 7 B). Expression of $Hmga2$ in LT-HSCs with WT $Jak2$ expanded cell numbers in culture (Fig. 7 B, phase contrast picture in top row) and led to the presence of megakaryocytes (Fig. 7 B, left). Co-expression of $Hmga2$ and V617F expanded the numbers of megakaryocytes. Similar results were also seen after retroviral transduction of $Lin28b$.

To determine the effects of forced expression of $Hmga2$ and $Lin28b$ in vivo, we retrovirally transduced FACS-sorted LT-HSCs from WT or V617F-expressing LT-HSCs and transplanted lethally irradiated C57BL/6 recipients (Fig. 7 C). We injected ~150 retrovirally transduced LT-HSCs together with 250,000 WT BM cells per mouse in three independent experiments. Because the retroviral vector contains a GFP cassette, the offspring of the transduced can be traced by the presence of GFP. Analysis of blood counts and GFP chimerism is shown at 8 wk after transplantation. Mice from all three experiments that displayed >5% GFP chimerism are shown in Fig. 7 C. Increased chimerism was observed in mice transplanted with $Hmga2$-transduced BM from WT mice, but the blood counts remained unchanged. $Hmga2$-transduced BM from V617F mice showed higher chimerism and higher platelet counts compared with vector control (MIGR). A trend toward increased hemoglobin and neutrophil counts was also noted. In contrast, forced expression of $Lin28b$ resulted in lower chimerism when BM from WT mice was used for transplantation. $Lin28b$ in combination with V617F expression resulted in very few recipient mice that reached any GFP chimerism, and only one mouse showed chimerism >5%. This mouse had normal blood counts. Thus, our functional data suggest that $Hmga2$ expression in $Ezh2$-deficient mice is linked to reduced deposition of H3K27me3 in its promoter. The increased expression of $Hmga2$ resulted in augmented cell production in vitro and in increased chimerism and platelet counts in vivo. $Lin28b$ had similar effects when transduced cells were cultured in vitro. However, in vivo $Lin28b$ did not show a synergistic effect with V617F, and its potential role in mediating the synergism between V617F and loss of $Ezh2$ is unclear. The synergism between V617F and loss of $Ezh2$ is likely to be mediated by a concerted action of several genes that are altered in their expression, and our data indicate that $Hmga2$ is one of these downstream targets.

Inhibitors of $Ezh2$ are currently in clinical trials for treatment of patients with lymphomas. Because our results show that genetic ablation of $Ezh2$ accelerated MPN in V617F-expressing mice, we tested whether pharmacological inhibition of Ezh2 might also have an MPN disease–promoting effect. We examined the effects of the Ezh2 inhibitor GSK126 in our previously described competitive transplantation model with V617F;GFP BM cells and WT competitor cells that allows monitoring of changes in mutant allele burden and in blood counts (Kubovcakova et al., 2013). Recipient mice transplanted with V617F;GFP received GSK126 by gavage for 34 d. Mice treated with the higher dosing regimen (150 mg/kg six times per week) displayed an increase in platelets (Fig. 7 D), mimicking the genetic ablation of Ezh2. We were unable to extend the duration of the treatment past 34 d because of toxicity (weight loss). Nevertheless, this result is consistent with the pronounced thrombocytosis when $Ezh2$ is genetically ablated in V617F-expressing mice. Caution should therefore be exercised in consideration of pharmacological inhibition of Ezh2 in the setting of MPN.
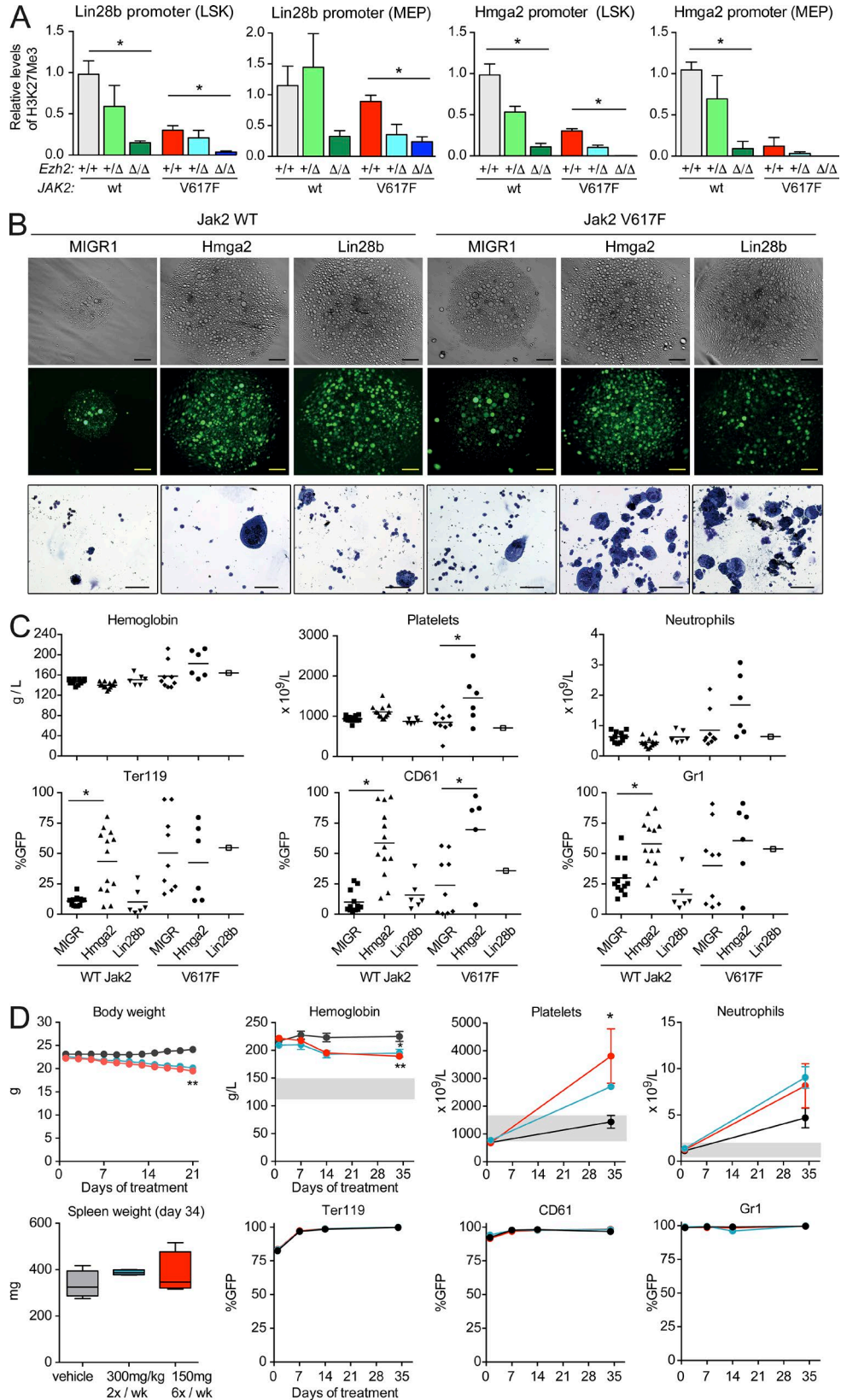
DISCUSSION

Our data provide evidence for functional synergism between $JAK2$-V617F and heterozygous or homozygous loss of $Ezh2$ in hematopoiesis in vivo. The MPN phenotype induced by V617F alone was accentuated in double mutant mice with V617F and heterozygous or homozygous loss of $Ezh2$. Peripheral blood counts, notably platelets and neutrophils, were increased, survival was reduced, and a higher degree of MF was observed in heterozygous $V617F;Ezh2^{+/\Delta}$ mice, and these alterations were even more pronounced in homozygous $V617F;Ezh2^{\Delta/\Delta}$ mice (Fig. 1). Loss of $Ezh2$ on a $Jak2$ WT background did not affect blood counts, survival, or histology.

Comparison of the progenitor and stem cell compartments between V617F and $V617F;Ezh2$ mutant mice revealed a slight increase of LT-HSCs in homozygous $V617F;Ezh2^{\Delta/\Delta}$ mice (Fig. 2 A), whereas a strong increase in MkPs and a decrease in erythroid precursors were noted (Fig. 2 B). These changes are in line with the alterations observed in peripheral blood of these mice. Although expansion of MEPs was observed in spleens of homozygous $V617F;Ezh2^{\Delta/\Delta}$ mice, this alteration may reflect increased activity of megakaryopoiesis

---

1490

Synergism between *Ezh2* deficiency and *JAK2*-V617F | Shimizu et al.

of this bipotent progenitor population. Loss of *Ezh2* on *Jak2* WT background had no significant effect on the progenitor and stem cell compartment compared with WT controls, except for an increase of MEPs in BM (Fig. 2 B).

Synergism between *JAK2*-V617F and heterozygous loss of *Ezh2* was also evident in BM transplantation experiments at limiting dilutions. BM grafts from heterozygous *V617F;Ezh2$^{+/\Delta}$* mice that contained on average only a single HSC engrafted at higher frequencies and showed more frequently a MPN phenotype in lethally irradiated recipients than grafts from *V617F* mice (Fig. 4 and Table 1). Although expression of *V617F* alone resulted in a decrease of functional HSC activity when 50 FACS-sorted LT-HSCs were transplanted in competition with WT BM cells, loss of *Ezh2* on *V617F* background restored the reconstitution capacity and increased disease initiation potential of FACS-sorted LT-HSCs (Fig. 5). The reduced efficiency of phenotypic LT-HSCs from *V617F* mice for long-term reconstitution in transplantation experiments was noted in our previous study and was accompanied by an expansion of stem cell activities in cells with lineage-intermediate Sca1$^+$ c-kit$^+$ immunophenotype (Lundberg et al., 2014b). Overall, the synergistic effects of *V617F* and loss of *Ezh2* manifested in expansion of the stem cell and progenitor cell compartment with increased reconstitution and MPN disease initiation potential and shift of differentiation toward megakaryopoiesis at the expense of erythropoiesis.

The effects of conditional *Ezh2* knockout in hematopoiesis have been previously studied. The tendency of increasing megakaryopoiesis was reported in conditional *Ezh2* knockout on a WT *Jak2* background. In one report, loss of *Ezh2* resulted in subtle thrombocytosis (Mochizuki-Kashio et al., 2011). Thrombocytopenia in *Mpl$^{-/-}$* mice was partially improved in *Mpl$^{-/-}$;Ezh2$^{\Delta/\Delta}$* double mutant mice (Majewski et al., 2010). We did not observe thrombocytosis in our *Ezh2$^{\Delta/\Delta}$* mice on a WT *Jak2* background, but we noted increased MEPs in BM and a trend toward more megakaryocytes (Fig. 2 B) as well as a shift toward increased platelet chimerism in *Ezh2$^{\Delta/\Delta}$* mice compared with WT controls (Fig. 5 F). Loss of *Ezh2* attenuated but did not prevent *MLL–AF9*–mediated acute myeloid leukemia (Neff et al., 2012). Although loss of *Ezh2* in the context of *V617F* accelerated disease, overexpression of

Ezh2 has also been implicated in the progression of various types of human cancers (reviewed by Sauvageau and Sauvageau [2010] and Margueron and Reinberg [2011]), and a recurrent gain of function mutation in *EZH2* (*EZH2*-Y641) has also been reported to occur in lymphomas (Morin et al., 2010; Yap et al., 2011). Paradoxically, overexpression of *Ezh2* also enhances HSC self-renewal (Kamminga et al., 2006) and results in a myeloproliferative disorder with leukocytosis and splenomegaly (Herrera-Merchan et al., 2012). These findings are difficult to reconcile and likely reflect the complex and cell type–dependent roles of PRC2 complex. Indeed, several compensatory mechanisms have been described that come into effect when *Ezh2* function is abolished, including compensation by Ezh1, as well as noncanonical PRC2 functions that do not depend on H3K27me3 (Xie et al., 2014).

Gene expression analysis in LT-HSC and MEP cells revealed strong effects of *V617F* over WT *Jak2* and also strong effects of homozygous loss of *Ezh2$^{\Delta/\Delta}$* (Fig. 6). In contrast, heterozygous *Ezh2$^{+/\Delta}$* had little influence on gene expression levels, despite showing functional synergism with *V617F* on the MPN phenotype in *V617F;Ezh2$^{+/\Delta}$* double mutant mice. Several genes highly up-regulated in MEPs from *Ezh2$^{\Delta/\Delta}$* mice on *Jak2* WT, as well as on a *V617F* background, have established functions in hematopoiesis, including *Lin28b*, a negative regulator of *let-7* microRNA biogenesis (Viswanathan et al., 2008; Piskounova et al., 2011), which is up-regulated in many human tumors and cancer cell lines (Viswanathan et al., 2009). The *Lin28b–let-7* pathway is involved in the regulation of HSC self-renewal in fetal and adult hematopoiesis (Copley et al., 2013). *Hmga2* is an established target of *let-7* and, when up-regulated, is linked to increased megakaryopoiesis and MF (Oguro et al., 2012). *Hmga2* is highly expressed in some patients with PMF (Andrieux et al., 2004). We also found *Hmga2* to be up-regulated in MEPs from *Ezh2$^{\Delta/\Delta}$* and *V617F;Ezh2$^{\Delta/\Delta}$* mice (Fig. 6 F) and also in granulocytes from MPN patients with homozygous loss of *EZH2* (Fig. 6 G). These data suggested a possible function of the *Lin28b–let7–Hmga2* axis in mediating the observed hyperproliferation of the megakaryocytic lineage and acceleration of MF in our mouse model.

ChIP-qPCR data demonstrated that the *Lin28b* and *Hmga2* promoters in LSK and MEP cells exhibit reduced

Figure 7. **Functional analysis of *Lin28b* and *Hmga2*.** (A) ChIP from LSK and MEP cells from mice with the indicated genotypes (*n* = 4 per each group) was performed with antibodies against H3K27me3 followed by qPCR analysis using primers for the promoter regions of *Lin28b* and *Hmga2*. Data pooled from two independent experiments are shown. (B) Growth of CD150$^+$CD48$^-$LSK (LT-HSC) transduced with the *Hmga2* or *Lin28b* retrovirus. 50 LT-HSCs were transduced with either the vector (MIGR) or *Hmga2* or *Lin28b* retrovirus and cultured in the presence of SCF and TPO. Colony picture and morphology of LT-HSCs at day 8 of culture are shown. The experiment was independently performed three times, and one representative picture is shown. Bars: (top and middle) 50 µm; (bottom) 100 µm. (C) Peripheral blood cell counts and donor chimerism of recipients repopulated with WT *Jak2* or *V617F* LT-HSCs transduced with the indicated vector. Recipient mice with >5% GFP positive chimerism are shown. The experiment was independently performed three times, and combined data are shown (*n* = 12 for MIGR transduction in WT LT-HSCs, *n* = 13 for *Hmga2* in WT LT-HSCs, *n* = 6 for *Lin28b* in WT LT-HSCs, *n* = 9 for MIGR transduction in *JAK2V617F* LT-HSCs, *n* = 6 for *Hmga2* transduction in *JAK2V617F* LT-HSCs, and *n* = 1 for *Lin28b* transduction in *JAK2V617F* LT-HSCs). Each dot represents data from one individual mouse. Horizontal lines indicate the mean of the values. (D) Pharmacological effect of Ezh2 inhibitor GSK-126. *V617F;GFP* BM cells were transplanted with WT BM cells in a 1:10 ratio. Recipient mice received GSK-126 by gavage at a dose of either 300 mg/kg twice per week (blue lines and dots) or 150 mg/kg six times per week (red lines and dots) for 34 d (*n* = 4 per group). This experiment was performed once. Statistical analysis was conducted using the Student's *t* test. *, P < 0.05; **, P < 0.01. Results are presented as means ± SEM.

H3K27me3 deposition upon *Ezh2* loss (Fig. 7 A), suggesting that both are normally repressed by *Ezh2*. Although forced expression of *Lin28b* in *V617F*-expressing cells increased cell numbers and megakaryocyte numbers during growth in vitro (Fig. 7 B), this effect was not observed in mice transplanted with retrovirally transduced BM cells in vivo (Fig. 7 C). In contrast, overexpressing *Hmga2* promoted megakaryopoiesis both in vitro and in vivo, suggesting that increased expression of *Hmga2* is a downstream event mediating synergism between *V617F* and loss of *Ezh2*.

Our data support the proposed tumor suppressor function of *EZH2* in patients with MPN. The synergism between mutant *JAK2*-V617F and reduced Ezh2 activity in hematopoiesis is evident in heterozygous *V617F;Ezh2$^{+/\Delta}$* mice, which is consistent with the finding that most MPN patients with *EZH2* mutations do not progress to homozygosity. The prospect of using *Ezh2* inhibitors in the context of MPN may carry the risk of aggravating the disease.

MATERIALS AND METHODS

Transgenic mice. Mice with Cre-recombinase–inducible human *JAK2*-V617F transgene were generated directly in the C57BL/6 background in our laboratory (Tiedt et al., 2008). These *V617F* mice were crossed with mice with a conditional *Ezh2* knockout allele, in which exons 16 and 17 are flanked by loxP sites (*Ezh2$^{fl/fl}$*; Neff et al., 2012) to generate double mutant mice (*V617F;Ezh2$^{fl/fl}$*). These mice were crossed with *MxCre* transgenic mice (Kühn et al., 1995) or *SclCre^{ER}* mice (Göthert et al., 2005) to obtain offspring that allow inducible deletion of the floxed *Ezh2* alleles and activation of the *V617F* transgene. *Ezh2$^{fl/fl}$*, *MxCre*, *SclCre^{ER}*, and *UBC-GFP* mice had been backcrossed into the C57BL/6 background for 12 generations, and the purity of the C57BL/6 background was verified using a 1449 SNP Illumina BeadChip panel and the SNaP-Map Software at the DartMouse Speed Congenic Core Facility at The Geisel School of Medicine at Dartmouth. Cre expression in *MxCre* mutant mice was induced by intraperitoneal injection of 300 µg pIpC three times every second day, and Cre expression in *SclCre* mutant mice was induced by intraperitoneal injection of 2 mg tamoxifen once daily for 4 wk, with a 1-wk break in the middle. The recipient C57BL/6 mice used for competitive transplantations were purchased from Janvier Labs. All mice in this study were kept under specific pathogen–free conditions with free access to food and water in accordance to Swiss Federal Regulations, and all experiments were performed in strict adherence to Swiss laws for animal welfare and approved by the Swiss Cantonal Veterinary Office of Basel-Stadt.

Competitive BM transplantations. For competitive transplantations, mice were intercrossed with the *UBC-GFP* strain, and whole BM or fractionated hematopoietic cells were used as donor cells. This system allows tracking donor-derived hematopoiesis (chimerism) in all hematopoietic lineages in recipient mice. Competitive whole BM transplantation was performed with 0.25×10^6 BM cells from 10-wk-old *SclCre* mutant mice without tamoxifen injection. Whole BM cells were transplanted intravenously into 10-wk-old female recipient mice (C57BL/6N) irradiated with 12 Gray (Gy), together with 0.75×10^6 BM cells of WT mice. Tamoxifen was injected for 5 wk, starting 8 wk after transplantation, with 1-wk break in the middle of the treatment. LT-HSC transplantations were performed with 50 purified LT-HSCs from *SclCre* mutant mice 12 wk after tamoxifen injection together with 10^6 BM cells of WT mice. LSK transplantation was performed with 1,500 purified LSK cells from MxCre mutant mice at 8 wk of age without pIpC injection together with 1.5×10^6 BM cells of WT mice. For competitive transplantations at limiting dilution, 20,000 total BM cells from *MxCre;GFP* or *MxCre;Ezh2$^{+/\Delta}$;GFP* donor mice 5 wk after pIpC injection were mixed with 2.0×10^6 WT BM cells (1:100 ratio) and transplanted into lethally irradiated female recipients. For competitive transplantations at limiting dilution from *MxCre;V617F;GFP* or *MxCre;V617F;Ezh2$^{+/\Delta}$;GFP* donor mice, 8,000 total BM cells were harvested 5 wk after pIpC injection and transplanted with 10^6 WT BM cells (1:250 ratio). Blood samples were taken every 6–8 wk to determine chimerism and for complete blood analysis. Secondary transplantations were performed with BM cells from primary recipients harvested at 30 wk after transplantation.

Purification of mouse LT–HSCs and MEP. Mouse LT-HSCs were purified from BM cells of *SclCre* mutant mice 12 wk after tamoxifen injection. BM mononuclear cells were stained with an allophycocyanin (APC)-conjugated anti–c-Kit antibodies (BioLegend). c-Kit–positive cells were isolated with goat anti–APC microbeads (Miltenyi Biotec) through an LS column (Miltenyi Biotec). The c-Kit–positive cells were further stained with antibody cocktail consisting of biotinylated anti–Gr-1, Mac-1, IL-7Rα, B220, CD4, CD8α, and Ter119 monoclonal antibodies (lineage-marker cocktail), PE-conjugated anti-CD150, PE-Cy7–conjugated anti-CD48, and brilliant violet 421 (BV421)–conjugated anti–Sca-1 antibodies. Biotinylated antibodies were detected with streptavidin-APC-Cy7 (BioLegend). Mouse MEPs were also purified from spleen cells of *SclCre* mutant mice 12 wk after tamoxifen injection. In brief, c-Kit–positive cells were isolated using PE-conjugated anti–c-Kit antibody and anti-PE microbeads with LS column (Miltenyi Biotec). The c-Kit–positive cells were further stained with lineage-marker cocktail followed by PE-Cy7–conjugated anti-CD16/32 (BioLegend), APC-conjugated anti-CD34 (BD), streptavidin-APC-Cy7, and BV421-conjugated anti–Sca-1 antibodies. Cell sorting was performed by Influx (BD), and results were analyzed with FlowJo software (Tree Star).

Transduction of mouse LT–HSCs and competitive repopulation assays. Recombinant retrovirus vectors, MIGR1-IRES-GFP, pMys-Hmga2-IRES-GFP, and pMys-Lin28b-IRES-GFP were provided by A. Iwama (Chiba University, Chuo-ku,

Chiba, Japan). LT-HSCs were sorted into 96-well microtiter plates coated with the recombinant fibronectin fragment CH-296 (RetroNectin; Takara Bio Inc.) at 300 cells/well and were incubated in StemSpan (STEMCELL Technologies) supplemented with 100 ng/ml mouse SCF (PeproTech) and 100 ng/ml human Tpo (PeproTech) for 24 h. The cells were transduced with a retrovirus vector at a multiplicity of infection of 800 in the presence of 10 μg/ml protamine sulfate (Sigma-Aldrich) and 1 μg/ml RetroNectin for 24 h. After transduction, cells were further incubated in in StemSpan supplemented with 10 ng/ml SCF and 10 ng/ml TPO. 150 LT-HSCs transduced with the indicated retrovirus were transplanted intravenously into 8-wk-old female C57BL/6 mice irradiated at a dose of 9.5 Gy, together with 2.5×10^5 BM competitor cells from 8-wk-old C57BL/6 mice.

Peripheral blood analysis. Blood was collected from the tail vein or by cardiac puncture, and complete blood counts (CBCs) were determined on an Advia120 Hematology Analyzer using Multispecies version 5.9.0-MS software (Bayer).

Flow cytometry analysis. The whole blood was stained with APC-conjugated anti-Ter119 and PE-conjugated anti-CD61 for erythrocyte and platelet analysis. White blood cells after RBC lyses were stained with PE-conjugated anti-CD8, PE-Cy7–conjugated anti-B220, APC-conjugated anti–Mac-1, APC-Cy7–conjugated anti-CD4, and Pacific blue (PB)–conjugated anti-Gr1 (BioLegend). Single cell suspensions from BM and spleen were stained with lineage-marker cocktail followed by FITC-conjugated anti-CD41, PE-conjugated anti-CD150, PE-Cy7–conjugated anti-CD48, APC-conjugated anti–c-Kit, BV421-conjugated anti–Sca-1, and streptavidin-APC-Cy7. For progenitor analysis, cells were stained with lineage-marker cocktail followed by FITC-conjugated anti-CD34 (BD), PE-conjugated anti-CD16/32, APC-conjugated anti–c-Kit, BV421-conjugated anti–Sca-1, and streptavidin-APC-Cy7 antibodies (BioLegend). For megakaryocytes and erythrocyte precursor analysis, cells were stained with FITC-conjugated anti-CD42c (Emfret), Dylight-647–conjugated anti-αIIbβ3 (CD41/61; Emfret), PE-conjugated anti-CD71, and APC-conjugated anti-Ter119. Analyses were performed on an LSRFortessa (BD) or CyAn ADP Analyzer (Beckman Coulter), and results were analyzed with FlowJo software.

Quantitative RT–PCR analysis. Total RNA was extracted from 0.5×10^6 BM cells from *SclCre* mutant mice 12 wk after tamoxifen injection using TRIzol solution (Thermo Fisher Scientific) and reverse transcribed by High Capacity cDNA reverse transcription kit (Thermo Fisher Scientific) with an oligo dT primer. Real-time qPCR was performed with 7500 Fast Real-Time PCR System (Thermo Fisher Scientific), using the Power SYBR Green PCR Master mix and normalized with mouse *Gusb*. Sequences of primers are as follows: 5′-ACTTACTGCTGGCACCGTCT-3′ and 5′-

GTTGAACAGAAAGCTGCACA-3′ for mouse *Ezh2* and 5′-ATAAGACGCATCAGAAGCCG-3′ and 5′-ACTCCT CACTGAACATGCGA-3′ for mouse Gusb. Total RNA from granulocytes of MPN patients were extracted and reverse transcribed using the same method (Lundberg et al., 2014a). Real-time qPCR was performed with 7500 Fast Real-Time PCR System, using the TaqMan gene expression system (Thermo Fisher Scientific) and normalized by human GUSB. The collection of blood samples was performed at the study center in Basel, Switzerland approved by the local Ethics Committee (Ethik Kommission Beider Basel) and at the study center in Florence, Italy according to a research protocol approved by local IRB in Florence (#2011/0014777 and #2015/0015136). Written informed consent was obtained from all patients in accordance with the Declaration of Helsinki. The diagnosis of MPN was established according to the revised criteria of the World Health Organization (Vardiman et al., 2009).

Western blotting. Total BM cells (20×10^6) from SclCre mutant mice 12 wk after tamoxifen injection were lysed and immediately boiled in 400 μl SDS sample buffer. The lysates were subjected to electrophoresis on NuPAGE 4–12% Bis-Tris Protein Gels (Invitrogen) and transferred to nitrocellulose membranes by Western blotting. The membranes were probed with antibodies against Ezh2 (CST), β-actin, histone H3 (Abcam), H3K27me27 (EMD Millipore), histone H2A (CST), and H2AK119Ub (CST). Signals were detected by HRP-conjugated anti–mouse IgG or HRP-conjugated anti–rabbit IgG antibodies, followed by ECL detection.

ChIP assay. ChIP was performed using a True MicroChIP kit from Diagenode. In brief, 10,000 LSK cells or MEP cells isolated by FACS were cross-linked with 1% formaldehyde for 8 min at room temperature and incubated for 5 min after addition of 0.125 M glycine. Cells were washed with PBS and lysed by lysis buffer, and sonicated to the DNA fragments were 200–500 bp by Bioruptor Pico (Diagenode). Immunoprecipitation was performed by using an anti-H3K27me27 (EMD Millipore), and DNA was purified using MicroChIP DiaPure columns (Diagenode). qPCR analysis was performed using Power SYBR Green PCR Master mix with 7500 Fast Real-Time PCR System (Thermo Fisher Scientific). Primer sequences are as follows: promoter region of *Hmga2*, 5′-CGAATCGTGGACAGGGACTT-3′ and 5′-GCCAAAGCGGCTGACAAA-3′; promoter region of *Lin28b*, 5′-GGGAGAGAGGAGAGCGGAAG-3′ and 5′-GGTGTGAACCCGGAAGTACAA-3′.

Next generation sequencing and bioinformatics analysis. Total RNA was isolated from 1,000 FACS-sorted LT-HSCs using Pico–Pure RNA isolation kit (ARCTURUS) or from 230,000 FACS-sorted MEP cells using TRIzol-LS solution. Total RNA was quality-checked on the Bioanalyzer instrument (Agilent Technologies) using the RNA 6000 Pico.

The library of LT-HSCs was prepared by using SMARTer Low Input RNA kit with Low Input Library Prep kit (Takara Bio Inc.). The library of MEPs was prepared using by TruSeq Stranded mRNA Library Prep kit (Illumina). Samples were pooled to equal molarity and run on the Fragment Analyzer for quality check and used for clustering on the NextSeq 500 instrument (Illumina). Samples were sequenced using the NextSeq 500 High Output kit 75-cycles (Illumina), and primary data analysis was performed with the Illumina RTA version 2.1.3 and bcl2fastq-2.16.0.10. Raw data were deposited in Gene Expression Omnibus under the accession no. GSE82074.

Reads were mapped against the mouse genome (version mm9; NCBI build 37) using the spliced-read aligner STAR (Dobin et al., 2013). The mean faction of mapped reads was 80%. All subsequent gene expression data analysis was performed within the R software (R Foundation for Statistical Computing). Raw reads and mapping quality were assessed by the qQCReport function from the R/Bioconductor software package QuasR (Gaidatzis et al., 2015). Expression of RefSeq genes was quantified by counting reads mapping into exons using the qCount function of QuasR. For gene expression visualization, the resulting count table was adjusted by library size and log transformed (log2 expression in figures). The full expression set was visualized as a heat map (unsupervised clustering of row and columns); it only includes genes that showed at least a 1.5 log2–fold change (relative to the mean) on an absolute scale in one of the samples and that were also significant (P ≤ 0.05) in one of the genotype comparisons. The heat map was generated using the NMF package (Gaujoux and Seoighe, 2010) with default clustering settings. For the PCA, genes were ordered by their absolute log2–fold change, and the top 1/4 ($n = 4708$) were retained for the analysis. PCA was performed with the R function "prcomp."

The R/Bioconductor software package edgeR (McCarthy et al., 2012) was used for detecting differentially expressed genes between genotypes. The model fitted by edgeR included both *Ezh2* and *Jak2* genotypes as well as their interaction effect and additionally adjusted for gender as a possible confounder. P-values for the contrasts between genotypes were calculated by likelihood ratio tests and adjusted for multiple testing by controlling the expected false discovery rate (Benjamini and Hochberg, 1995). Competitive gene set enrichment analysis was performed on all categories of the Molecular Signature Database (MSigDB) using the function CAMERA of the edgeR package. The self-contained gene set testing on gene signature of fetal liver HSCs (Copley et al., 2013) was conducted using the function ROAST of the edgeR package.

Statistical analysis. Results are presented as means ± SEM. To assess the statistical significance among individual cohorts, one-way ANOVA with subsequent Bonferroni's post-hoc multiple comparison test (Prism version 6 software; Graph-Pad Software) or unpaired Student's *t* test was used. P ≤ 0.05 was considered significant.

Online supplemental material. Table S1, available as an Excel file, contains the complete gene list of differentially expressed transcripts found in LT-HSCs. Table S2, available as an Excel file, contains the complete gene list of differentially expressed transcripts found in MEP cells. Online supplemental material is available at http://www.jem.org/cgi/content/full/jem.20151136/DC1.

REFERENCES
Andrieux, J., J.L. Demory, B. Dupriez, S. Quief, I. Plantier, C. Roumier, F. Bauters, J.L. Laï, and J.P. Kerckaert. 2004. Dysregulation and overexpression of HMGA2 in myelofibrosis with myeloid metaplasia. *Genes Chromosomes Cancer.* 39:82–87. http://dx.doi.org/10.1002/gcc.10297

Barosi, G., G. Viarengo, A. Pecci, V. Rosti, G. Piaggio, M. Marchetti, and F. Frassoni. 2001. Diagnostic and clinical relevance of the number of circulating CD34$^+$ cells in myelofibrosis with myeloid metaplasia. *Blood.* 98:3249–3255. http://dx.doi.org/10.1182/blood.V98.12.3249

Baxter, E.J., L.M. Scott, P.J. Campbell, C. East, N. Fourouclas, S. Swanton, G.S. Vassiliou, A.J. Bench, E.M. Boyd, N. Curtin, et al. Cancer Genome Project. 2005. Acquired mutation of the tyrosine kinase JAK2 in human myeloproliferative disorders. *Lancet.* 365:1054–1061. http://dx.doi.org/10.1016/S0140-6736(05)74230-6

Bejar, R., K. Stevenson, O. Abdel-Wahab, N. Galili, B. Nilsson, G. Garcia-Manero, H. Kantarjian, A. Raza, R.L. Levine, D. Neuberg, and B.L. Ebert. 2011. Clinical effect of point mutations in myelodysplastic syndromes. *N. Engl. J. Med.* 364:2496–2506. http://dx.doi.org/10.1056/NEJMoa1013343

Benjamini, Y., and Y. Hochberg. 1995. Controlling the false discovery rate: A practical and powerful approach to multiple testing. *J. R. Stat. Soc. Series B Stat. Methodol.* 57:289–300.

Copley, M.R., S. Babovic, C. Benz, D.J. Knapp, P.A. Beer, D.G. Kent, S. Wohrer, D.Q. Treloar, C. Day, K. Rowe, et al. 2013. The Lin28b–let-7–Hmga2 axis determines the higher self-renewal potential of fetal haematopoietic stem cells. *Nat. Cell Biol.* 15:916–925. http://dx.doi.org/10.1038/ncb2783

Dobin, A., C.A. Davis, F. Schlesinger, J. Drenkow, C. Zaleski, S. Jha, P. Batut, M. Chaisson, and T.R. Gingeras. 2013. STAR: ultrafast universal RNA-seq aligner. *Bioinformatics.* 29:15–21. http://dx.doi.org/10.1093/bioinformatics/bts635

1494

Synergism between *Ezh2* deficiency and *JAK2*-V617F | Shimizu et al.

Ernst, T., A.J. Chase, J. Score, C.E. Hidalgo-Curtis, C. Bryant, A.V. Jones, K. Waghorn, K. Zoi, F.M. Ross, A. Reiter, et al. 2010. Inactivating mutations of the histone methyltransferase gene EZH2 in myeloid disorders. *Nat. Genet.* 42:722–726. http://dx.doi.org/10.1038/ng.621

Gaidatzis, D., A. Lerch, F. Hahne, and M.B. Stadler. 2015. QuasR: quantification and annotation of short reads in R. *Bioinformatics.* 31:1130–1132. http://dx.doi.org/10.1093/bioinformatics/btu781

Gaujoux, R., and C. Seoighe. 2010. A flexible R package for nonnegative matrix factorization. *BMC Bioinformatics.* 11:367. http://dx.doi.org/10.1186/1471-2105-11-367

Gerstung, M., A. Pellagatti, L. Malcovati, A. Giagounidis, M.G. Porta, M. Jädersten, H. Dolatshad, A. Verma, N.C. Cross, P. Vyas, et al. 2015. Combining gene mutation with gene expression data improves outcome prediction in myelodysplastic syndromes. *Nat. Commun.* 6:5901. http://dx.doi.org/10.1038/ncomms6901

Göthert, J.R., S.E. Gustin, M.A. Hall, A.R. Green, B. Göttgens, D.J. Izon, and C.G. Begley. 2005. In vivo fate-tracing studies using the Scl stem cell enhancer: embryonic hematopoietic stem cells significantly contribute to adult hematopoiesis. *Blood.* 105:2724–2732. http://dx.doi.org/10.1182/blood-2004-08-3037

Guglielmelli, P., F. Biamonte, J. Score, C. Hidalgo-Curtis, F. Cervantes, M. Maffioli, T. Fanelli, T. Ernst, N. Winkelman, A.V. Jones, et al. 2011. EZH2 mutational status predicts poor survival in myelofibrosis. *Blood.* 118:5227–5234. http://dx.doi.org/10.1182/blood-2011-06-363424

Herrera-Merchan, A., L. Arranz, J.M. Ligos, A. de Molina, O. Dominguez, and S. Gonzalez. 2012. Ectopic expression of the histone methyltransferase Ezh2 in haematopoietic stem cells causes myeloproliferative disease. *Nat. Commun.* 3:623. http://dx.doi.org/10.1038/ncomms1623

Hirabayashi, Y., N. Suzki, M. Tsuboi, T.A. Endo, T. Toyoda, J. Shinga, H. Koseki, M. Vidal, and Y. Gotoh. 2009. Polycomb limits the neurogenic competence of neural precursor cells to promote astrogenic fate transition. *Neuron.* 63:600–613. http://dx.doi.org/10.1016/j.neuron.2009.08.021

James, C., V. Ugo, J.P. Le Couédic, J. Staerk, F. Delhommeau, C. Lacout, L. Garçon, H. Raslova, R. Berger, A. Bennaceur-Griscelli, et al. 2005. A unique clonal JAK2 mutation leading to constitutive signalling causes polycythaemia vera. *Nature.* 434:1144–1148. http://dx.doi.org/10.1038/nature03546

Kamminga, L.M., L.V. Bystrykh, A. de Boer, S. Houwer, J. Douma, E. Weersing, B. Dontje, and G. de Haan. 2006. The Polycomb group gene Ezh2 prevents hematopoietic stem cell exhaustion. *Blood.* 107:2170–2179. http://dx.doi.org/10.1182/blood-2005-09-3585

Klampfl, T., H. Gisslinger, A.S. Harutyunyan, H. Nivarthi, E. Rumi, J.D. Milosevic, N.C. Them, T. Berg, B. Gisslinger, D. Pietra, et al. 2013. Somatic mutations of calreticulin in myeloproliferative neoplasms. *N. Engl. J. Med.* 369:2379–2390. http://dx.doi.org/10.1056/NEJMoa1311347

Kralovics, R., F. Passamonti, A.S. Buser, S.S. Teo, R. Tiedt, J.R. Passweg, A. Tichelli, M. Cazzola, and R.C. Skoda. 2005. A gain-of-function mutation of JAK2 in myeloproliferative disorders. *N. Engl. J. Med.* 352:1779–1790. http://dx.doi.org/10.1056/NEJMoa051113

Kubovcakova, L., P. Lundberg, J. Grisouard, H. Hao-Shen, V. Romanet, R. Andraos, M. Murakami, S. Dirnhofer, K.U. Wagner, T. Radimerski, and R.C. Skoda. 2013. Differential effects of hydroxyurea and INC424 on mutant allele burden and myeloproliferative phenotype in a JAK2-V617F polycythemia vera mouse model. *Blood.* 121:1188–1199. http://dx.doi.org/10.1182/blood-2012-03-415646

Kühn, R., F. Schwenk, M. Aguet, and K. Rajewsky. 1995. Inducible gene targeting in mice. *Science.* 269:1427–1429. http://dx.doi.org/10.1126/science.7660125

Levine, R.L., M. Wadleigh, J. Cools, B.L. Ebert, G. Wernig, B.J. Huntly, T.J. Boggon, I. Wlodarska, J.J. Clark, S. Moore, et al. 2005. Activating mutation in the tyrosine kinase JAK2 in polycythemia vera, essential thrombocythemia, and myeloid metaplasia with myelofibrosis. *Cancer Cell.* 7:387–397. http://dx.doi.org/10.1016/j.ccr.2005.03.023

Li, J., D.G. Kent, E. Chen, and A.R. Green. 2011. Mouse models of myeloproliferative neoplasms: JAK of all grades. *Dis. Model. Mech.* 4:311–317. http://dx.doi.org/10.1242/dmm.006817

Lundberg, P., A. Karow, R. Nienhold, R. Looser, H. Hao-Shen, I. Nissen, S. Girsberger, T. Lehmann, J. Passweg, M. Stern, et al. 2014a. Clonal evolution and clinical correlates of somatic mutations in myeloproliferative neoplasms. *Blood.* 123:2220–2228. http://dx.doi.org/10.1182/blood-2013-11-537167

Lundberg, P., H. Takizawa, L. Kubovcakova, G. Guo, H. Hao-Shen, S. Dirnhofer, S.H. Orkin, M.G. Manz, and R.C. Skoda. 2014b. Myeloproliferative neoplasms can be initiated from a single hematopoietic stem cell expressing JAK2-V617F. *J. Exp. Med.* 211:2213–2230. http://dx.doi.org/10.1084/jem.20131371

Majewski, I.J., M.E. Ritchie, B. Phipson, J. Corbin, M. Pakusch, A. Ebert, M. Busslinger, H. Koseki, Y. Hu, G.K. Smyth, et al. 2010. Opposing roles of polycomb repressive complexes in hematopoietic stem and progenitor cells. *Blood.* 116:731–739. http://dx.doi.org/10.1182/blood-2009-12-260760

Margueron, R., and D. Reinberg. 2011. The Polycomb complex PRC2 and its mark in life. *Nature.* 469:343–349. http://dx.doi.org/10.1038/nature09784

McCarthy, D.J., Y. Chen, and G.K. Smyth. 2012. Differential expression analysis of multifactor RNA-Seq experiments with respect to biological variation. *Nucleic Acids Res.* 40:4288–4297. http://dx.doi.org/10.1093/nar/gks042

Mochizuki-Kashio, M., Y. Mishima, S. Miyagi, M. Negishi, A. Saraya, T. Konuma, J. Shinga, H. Koseki, and A. Iwama. 2011. Dependency on the polycomb gene Ezh2 distinguishes fetal from adult hematopoietic stem cells. *Blood.* 118:6553–6561. http://dx.doi.org/10.1182/blood-2011-03-340554

Morin, R.D., N.A. Johnson, T.M. Severson, A.J. Mungall, J. An, R. Goya, J.E. Paul, M. Boyle, B.W. Woolcock, F. Kuchenbauer, et al. 2010. Somatic mutations altering EZH2 (Tyr641) in follicular and diffuse large B-cell lymphomas of germinal-center origin. *Nat. Genet.* 42:181–185. http://dx.doi.org/10.1038/ng.518

Nangalia, J., C.E. Massie, E.J. Baxter, F.L. Nice, G. Gundem, D.C. Wedge, E. Avezov, J. Li, K. Kollmann, D.G. Kent, et al. 2013. Somatic CALR mutations in myeloproliferative neoplasms with nonmutated JAK2. *N. Engl. J. Med.* 369:2391–2405. http://dx.doi.org/10.1056/NEJMoa1312542

Neff, T., A.U. Sinha, M.J. Kluk, N. Zhu, M.H. Khattab, L. Stein, H. Xie, S.H. Orkin, and S.A. Armstrong. 2012. Polycomb repressive complex 2 is required for MLL-AF9 leukemia. *Proc. Natl. Acad. Sci. USA.* 109:5028–5033. http://dx.doi.org/10.1073/pnas.1202258109

O'Carroll, D., S. Erhardt, M. Pagani, S.C. Barton, M.A. Surani, and T. Jenuwein. 2001. The polycomb-group gene Ezh2 is required for early mouse development. *Mol. Cell. Biol.* 21:4330–4336. http://dx.doi.org/10.1128/MCB.21.13.4330-4336.2001

Oguro, H., J. Yuan, S. Tanaka, S. Miyagi, M. Mochizuki-Kashio, H. Ichikawa, S. Yamazaki, H. Koseki, H. Nakauchi, and A. Iwama. 2012. Lethal myelofibrosis induced by Bmi1-deficient hematopoietic cells unveils a tumor suppressor function of the polycomb group genes. *J. Exp. Med.* 209:445–454. http://dx.doi.org/10.1084/jem.20111709

Pardanani, A.D., R.L. Levine, T. Lasho, Y. Pikman, R.A. Mesa, M. Wadleigh, D.P. Steensma, M.A. Elliott, A.P. Wolanskyj, W.J. Hogan, et al. 2006. MPL515 mutations in myeloproliferative and other myeloid disorders: a study of 1182 patients. *Blood.* 108:3472–3476. http://dx.doi.org/10.1182/blood-2006-04-018879

Pikman, Y., B.H. Lee, T. Mercher, E. McDowell, B.L. Ebert, M. Gozo, A. Cuker, G. Wernig, S. Moore, I. Galinsky, et al. 2006. MPLW515L is a novel

somatic activating mutation in myelofibrosis with myeloid metaplasia. *PLoS Med*. 3:e270. http://dx.doi.org/10.1371/journal.pmed.0030270

Piskounova, E., C. Polytarchou, J.E. Thornton, R.J. LaPierre, C. Pothoulakis, J.P. Hagan, D. Iliopoulos, and R.I. Gregory. 2011. Lin28A and Lin28B inhibit let-7 microRNA biogenesis by distinct mechanisms. *Cell*. 147:1066–1079. http://dx.doi.org/10.1016/j.cell.2011.10.039

Sauvageau, M., and G. Sauvageau. 2010. Polycomb group proteins: multi-faceted regulators of somatic stem cells and cancer. *Cell Stem Cell*. 7:299–313. http://dx.doi.org/10.1016/j.stem.2010.08.002

Schaefer, B.C., M.L. Schaefer, J.W. Kappler, P. Marrack, and R.M. Kedl. 2001. Observation of antigen-dependent CD8⁺ T-cell/ dendritic cell interactions in vivo. *Cell. Immunol*. 214:110–122. http://dx.doi.org/10.1006/cimm.2001.1895

Tefferi, A., J. Thiele, and J.W. Vardiman. 2009. The 2008 World Health Organization classification system for myeloproliferative neoplasms: order out of chaos. *Cancer*. 115:3842–3847. http://dx.doi.org/10.1002/cncr.24440

Tiedt, R., H. Hao-Shen, M.A. Sobas, R. Looser, S. Dirnhofer, J. Schwaller, and R.C. Skoda. 2008. Ratio of mutant JAK2-V617F to wild-type Jak2 determines the MPD phenotypes in transgenic mice. *Blood*. 111:3931–3940. http://dx.doi.org/10.1182/blood-2007-08-107748

Vainchenker, W., F. Delhommeau, S.N. Constantinescu, and O.A. Bernard. 2011. New mutations and pathogenesis of myeloproliferative neoplasms.

Blood. 118:1723–1735. http://dx.doi.org/10.1182/blood-2011-02-292102

Vardiman, J.W., J. Thiele, D.A. Arber, R.D. Brunning, M.J. Borowitz, A. Porwit, N.L. Harris, M.M. Le Beau, E. Hellström-Lindberg, A. Tefferi, and C.D. Bloomfield. 2009. The 2008 revision of the World Health Organization (WHO) classification of myeloid neoplasms and acute leukemia: rationale and important changes. *Blood*. 114:937–951. http://dx.doi.org/10.1182/blood-2009-03-209262

Viswanathan, S.R., G.Q. Daley, and R.I. Gregory. 2008. Selective blockade of microRNA processing by Lin28. *Science*. 320:97–100. http://dx.doi.org/10.1126/science.1154040

Viswanathan, S.R., J.T. Powers, W. Einhorn, Y. Hoshida, T.L. Ng, S. Toffanin, M. O'Sullivan, J. Lu, L.A. Phillips, V.L. Lockhart, et al. 2009. Lin28 promotes transformation and is associated with advanced human malignancies. *Nat. Genet*. 41:843–848. http://dx.doi.org/10.1038/ng.392

Xie, H., J. Xu, J.H. Hsu, M. Nguyen, Y. Fujiwara, C. Peng, and S.H. Orkin. 2014. Polycomb repressive complex 2 regulates normal hematopoietic stem cell function in a developmental-stage-specific manner. *Cell Stem Cell*. 14:68–80. http://dx.doi.org/10.1016/j.stem.2013.10.001

Yap, D.B., J. Chu, T. Berg, M. Schapira, S.W. Cheng, A. Moradian, R.D. Morin, A.J. Mungall, B. Meissner, M. Boyle, et al. 2011. Somatic mutations at EZH2 Y641 act dominantly through a mechanism of selectively altered PRC2 catalytic activity, to increase H3K27 trimethylation. *Blood*. 117:2451–2459. http://dx.doi.org/10.1182/blood-2010-11-321208